RIG-I and PKR, but not stress granules, mediate the pro-inflammatory response to Yellow fever virus

Guillaume Beauclair[1], Felix Streicher[1], Daniela Bruni[1], Ségolène Gracias[1], Salomé Bourgeau[1], Laura Sinigaglia[1], Takashi Fujita[2], Eliane F. Meurs[1], Frédéric Tangy[1] and Nolwenn Jouvenet[1]*

[1] *Viral Genomics and Vaccination Unit, Institut Pasteur, UMR3569 CNRS, 75015 Paris, France*

[2] *Department of Virus Research, Institute for Frontier Life and Medical Sciences, Kyoto University, Kyoto, Japan.*

Short title: Innate response against YFV in liver cells

*Corresponding author: nolwenn.jouvenet@pasteur.fr

Abstract

Yellow fever virus (YFV) is an RNA virus primarily targeting the liver. Severe YF cases are responsible for hemorrhagic fever, plausibly precipitated by excessive pro-inflammatory cytokine response. Pathogen recognition receptors (PRRs), such as the cytoplasmic RIG-I-like receptors (RLRs), and the viral RNA sensor PKR are known to initiate a pro-inflammatory response upon recognition of viral genomes. Here, we sought to reveal the main determinants responsible for the acute cytokine expression occurring in human hepatocytes following YFV infection. Using a RIG-I-defective human hepatoma cell line, we found that RIG-I largely contributes to cytokine secretion upon YFV infection. In infected RIG-I-proficient hepatoma cells, RIG-I was localized in stress granules. These granules are large aggregates of stalled translation preinitiation complexes known to concentrate RLRs and PKR, and are so far recognized as hubs orchestrating RNA virus sensing. Using PKR-deficient hepatoma cells, we found that PKR contributes to both stress granule formation and cytokine induction upon YFV infection. However, stress granules disruption did not affect the cytokine response to YFV infection, as assessed by siRNA-knockdown-mediated inhibition of stress granule assembly. Finally, no viral RNA was detected in stress granules using a fluorescence *in situ* hybridization approach coupled with immunofluorescence. Our findings suggest that both RIG-I and PKR mediate pro-inflammatory cytokine induction in YFV-infected hepatocytes, in a stress granule-independent manner. Therefore, by showing the uncoupling of the early cytokine response from the stress granules formation, our model challenges the current view by which stress granules are required for the mounting of the acute antiviral response.

Importance

Yellow fever is a mosquito-borne acute hemorrhagic disease caused by yellow fever virus (YFV). The mechanisms responsible for its pathogenesis remain largely unknown, although increased inflammation has been linked to worsened outcome. YFV targets the liver, where it primarily infects hepatocytes. We found that two RNA-sensing proteins, RIG-I and PKR, participate in the induction of pro-inflammatory mediators

54 in human hepatocytes infected with YFV. We show that YFV infection promotes the formation of
55 cytoplasmic structures, termed stress granules, in a PKR-, but not RIG-I-dependent manner. Whilst stress
56 granules were previously postulated to be essential platforms for immune activation, we found that they are
57 not required for pro-inflammatory mediators' production upon YFV infection. Collectively, our work
58 uncovered molecular events triggered by the replication of YFV, which could prove instrumental in
59 clarifying the pathogenesis of the disease, with possible repercussions on disease management.
60
61

62 **Introduction**

63 Flaviviruses are a group of more than seventy enveloped RNA viruses that can cause serious diseases in
64 humans and animals (1, 2). They have provided some of the most important examples of emerging or
65 resurging diseases of global significance. Most flaviviruses, such as dengue virus (DENV), yellow fever
66 virus (YFV) and Zika virus (ZIKV), are arthropod-borne viruses transmitted to vertebrate hosts by
67 mosquitoes or ticks (1). YFV is the prototype and eponymous virus of the Flavivirus genus. It is a small
68 (40–60 nm), enveloped virus harboring a single positive-strand RNA genome of 11 kb. The genome
69 encodes a polyprotein that is cleaved co- and post-translationally into three structural proteins: capsid
70 (C), membrane precursor (prM) and envelope (E), and seven non-structural (NS) proteins (NS1, NS2a,
71 NS2b, NS3, NS4a, NS4b, and NS5). The C, prM, and E proteins are incorporated into the virions, while
72 NS proteins are found only in infected cells (3). NS proteins coordinate RNA replication, viral assembly
73 and modulate innate immune responses, while the structural proteins constitute the virion.

74 YFV is endemic in the tropical regions of sub-Saharan Africa and South America. The reference
75 strain Asibi was isolated in 1927 in West Africa from the blood of a human patient. The vaccine strain
76 17D was developed empirically in the 1930s, by passaging the Asibi strain in rhesus macaques, mouse
77 and chicken embryonic tissues (4). 17D is one of the most effective vaccines ever generated. It has been
78 used safely and effectively on more than 600 million individuals over the past 70 years (4). However,
79 due to poor vaccine coverage and vaccine shortages, the virus continues to cause disease in endemic areas,
80 as illustrated by recent outbreaks in Angola and Brazil (5, 6).

81 Yellow fever (YF) pathogenesis is viscerotropic in humans, with viral replication in the liver critical
82 to the establishment of the disease (3). Severe YF is responsible for multi-system organ failure and viral
83 hemorrhagic fever resulting in up to 50% fatality. Similar to Ebola hemorrhagic fever, cytokine dysregulation
84 is thought to result in endothelial damage, disseminated intravascular coagulation and circulatory shock
85 observed in the terminal stage of the disease. Viral hemorrhagic fever is considered as an illness
86 precipitated by excessive pro-inflammatory cytokine response ('cytokine storm') (7, 8). Almost any cell
87 type in the body can produce pro-inflammatory cytokines in response to various stimuli, such as a viral
88 infection (9). The pattern of cytokine expression in response to infection with pathogenic strains of YFV
89 has been described both in humans and in rhesus macaques. Studies performed on patients during a YF
90 outbreak in the Republic of Guinea in 2000 showed that excessive production of pro-inflammatory
91 cytokines, such as IL6 and TNFα, correlates with high viremia and disease outcome (10). The levels of
92 these two cytokines were statistically higher in patients with fatal hemorrhagic fever than in patients
93 who survived. Similar findings were obtained with rhesus macaques infected with the strain Dakar-
94 HD1279 (11). The animals died of hemorrhagic fever within five days. These studies also suggest that
95 pro-inflammatory cytokines might be produced by injured organs, especially the liver, and not by cells
96 circulating in the blood (11).
97 Upon viral infection, the cytokine response is initiated by the recognition of viral genomes and viral
98 replication intermediates by pathogen recognition receptors (PRRs) (12), such as the ubiquitously
99 expressed cytoplasmic RIG-I-like receptors (RLRs). Three RLRs have been identified in vertebrates:
100 melanoma differentiation-associated gene 5 (MDA5), laboratory of genetics and physiology 2 (LGP2)
101 and retinoic acid inducible gene 1 (RIG-I) (13). Upon binding to viral nucleic acids, MDA5 and RIG-I
102 undergo a conformational change, which allows interaction with the adaptor protein MAVS and
103 subsequent recruitment of signaling complexes that comprises protein kinases such as TBK1, IKKα,
104 IKKβ and IKKε (14). These events lead to the activation and nuclear translocation of the transcription
105 factors IRF3 and NF-κB, which stimulate the rapid expression of pro-inflammatory cytokines and type
106 I interferons (IFNs).
107 RIG-I plays an important role in initiating the IFN-mediated antiviral response against DENV and
108 ZIKV (15–18). Induction of cytokines upon infection with the vaccine strain of YFV is also mediated

109 by RIG-I in plasmacytoid dendritic cells (19). Whether RIG-I contributes to cytokine production in cells
110 infected with wild-type YFV strains is not known.

111 The subcellular localization where RIG-I interacts with its ligands is not well described. Upon
112 infection with influenza A virus lacking its non-structural protein 1 (IAVΔNS1), Newcastle disease
113 virus or Sendai virus (20–23), RIG-I accumulates in cytoplasmic foci. Disruption of these foci, which
114 have been identified as stress granules, reduced the abundance of *IFNB* mRNAs in IAVΔNS1-infected
115 cells (20). Thus, stress granules may be important for RIG-I signaling and could serve as a platform for
116 viral RNA sensing. Moreover, other viral nucleic sensors, such as MDA5 (24), LGP2 (25) and cGAS
117 (26), are also concentrated in stress granules. Finally, numerous viruses interfere with stress granule
118 formation, *via*, for instance, the cleavage of one of their core components by a viral protease. Thus,
119 accumulation of viral sensors in stress granules and viral counteraction mechanisms suggest that these
120 granules act as hubs that coordinate foreign nucleic acid sensing (27, 28).

121 Stress granules are non-membranous cytoplasmic structures that concentrate translationally stalled
122 mRNAs and proteins (29). Their assembly is triggered by sensing distinct types of stress, including viral
123 infection, by one of four kinases, resulting in phosphorylation of the eukaryotic initiation factor 2α
124 (eIF2α). These kinases are: the heme-regulated inhibitor (HRI), which is activated by heat shock or
125 oxidative stress (*e.g*. by reactive oxygen species (ROS) produced upon treatment with sodium arsenite);
126 general control non-depressible protein 2 (GCN2), which reacts to UV-induced damage or amino acid
127 deprivation; dsRNA-sensing protein kinase R (PKR); and PKR-like endoplasmatic reticulum (ER)
128 kinase (PERK), which is activated upon ER stress (29). Stress granule assembly does not only arrest the
129 host translation machinery, but also heavily disturb viral translation, which is further evidence for their
130 antiviral nature (27, 28, 30). Here, we investigated the role of RIG-I, PKR and stress granules in the
131 induction of inflammatory cytokines upon infection of hepatoma cells with YFV.

132

133 **Results**

134 **The Asibi strain of YFV triggers the production of pro-inflammatory cytokines in hepatoma cells**
135 **through RIG-I, IRF3 and NF-κB**

136 We examined whether the YFV reference strain Asibi could trigger the expression of pro-
137 inflammatory cytokines in human hepatoma cells through the RIG-I signaling pathway. Huh7 and
138 Huh7.5 cells, a clone derived from Huh7 that expresses an inactive form of the viral sensor RIG-I (31),
139 were infected with the Asibi strain for 24 or 48 hours. The abundances of *TNFA*, *IL6* and *IFNB* mRNAs
140 increased over time with infection in Huh7 cells, while being significantly lower in Huh7.5 cells at 48
141 hours post-infection (hpi) (**Fig. 1A-C**). We noticed that Huh7.5 cells infected for 48 hours produced
142 approximately three-fold more viral RNA than Huh7 cells infected for the same amount of time (**Fig.**
143 **1D)**. Albeit not statistically significant, this modest effect was reproducible (**Fig. 1D)** and suggests that
144 absence of RIG-I signaling favors viral replication. Huh7 cells secreted around 10 to 20 pg/ml of IL6
145 and TNFα protein after 48 hours of infection, but not after 24 hpi (**Fig. 1E, F**). By contrast, the amount
146 of IL6 and TNFα protein secreted by cells expressing the inactive form of RIG-I was below the detection
147 limit of the ELISA (**Fig 1E, F**). These data suggest that Asibi infection triggers the induction and
148 secretion of pro-inflammatory cytokines in a RIG-I-dependent manner in human hepatoma cells.
149 By Western blot analysis, we found that IRF3 was activated in Huh7 cells infected with Asibi for
150 24 or 48 hours, but not in non-infected cells (**Fig. 1G**). The level of IRF3 phosphorylation was higher
151 at 48 than at 24 hpi, despite the total protein abundance being similar at these two points in time (**Fig.**
152 **1G**). IRF3 was not phosphorylated in Huh7.5 cells infected with Asibi (**Fig. 1G**). IκBα is a negative
153 regulator of the NF-κB pathway: its degradation triggers the nuclear translocation of the NF-κB subunits
154 p65 and p50. IκBα was degraded in Huh7 cells infected for 48 hours (**Fig. 1G**). Slightly more of the
155 viral protein NS4b was produced in Huh7.5 cells than in Huh7 cells upon 48 hours of Asibi infection
156 (**Fig. 1G**), which is consistent with the RT-qPCR analysis (**Fig. 1D**). These experiments indicate that
157 both IRF3 and NF-κB are activated during Asibi infection of human hepatoma cells and that RIG-I
158 contributes to IRF3 activation.
159 Immunofluorescence analysis revealed that IRF3 was detectable exclusively in the cytosol of 100%
160 of uninfected cells, whereas it was found both in the cytosol and the nucleus of around 50% of cells
161 infected for 24 hours (**Fig. 1H**). Infected cells were identified with antibodies recognizing dsRNA
162 structures, including probably viral replicative intermediates (**Fig. 1H**). Similar quantification showed

163 that around 3% of uninfected cells exhibited nuclei positive for the NF-κB subunit p65 whereas around
164 65% of Asibi-infected cells showed nuclei positive for p65 (**Fig. 1I**).
165 Together, these results suggest that both the NF-κB and the IRF3 pathways are activated upon Asibi
166 infection of human hepatoma cells and their initiation is dependent on RIG-I.
167
168 **RIG-I localizes in stress granules in human and monkey cells infected with YFV**
169 Having determined that RIG-I is important for mediating a cytokine response in Huh7 cells infected
170 with Asibi (**Fig. 1**), we then investigated its subcellular localization. The distribution of the RIG-I signal
171 was found to be weak and diffuse in the cytosol of uninfected Huh7 cells (**Fig. 2A**), which is consistent
172 with data reported for unstimulated HeLa cells (20). After infection with Asibi for 24 hours, RIG-I
173 accumulated in cytosolic foci (**Fig. 2A**). Since RIG-I was previously shown to localize in stress granules
174 in HeLa cells infected with several types of viruses (20–23), the Huh7 cells were also stained with the
175 stress granule marker TIA-1 related protein (TIAR). In non-infected cells, the TIAR signal was weak
176 and diffused in the cytoplasm and in the nucleus of the cells. In infected cells, TIAR was redistributed
177 into cytoplasmic foci (**Fig. 2A**). The RIG-I structures present in infected cells co-localized with TIAR
178 foci (**Fig. 2A**, zoom images for details), suggesting that RIG-I is recruited to stress granules upon
179 infection. The intensity profiles of individual foci confirmed that the RIG-I signal and the TIAR signal
180 overlapped (**Fig. 2A**, right panels). These profiles also revealed that dsRNAs seemed to be excluded
181 from stress granules (**Fig. 2A**).
182 To follow the formation of stress granules in infected cells, the localization of TIAR and RAS
183 GTPase-activating protein SH3 domain-binding protein 1 and 2 (G3BP), which are canonical stress
184 granule markers (29), were examined in Huh7 cells infected with Asibi for over time (**Fig. 2B**). Infected
185 cells were identified by the presence of the viral protein NS4b (**Fig. 2B**). TIAR and G3BP were diffuse
186 in non-infected cells. They remained diffuse until 12 hpi, where 16% of cells were determined positive
187 for NS4b. Fifteen hours after infection, around 80% of cells were infected and around 40% of the total
188 number of cells exhibited TIAR- and G3BP-positive foci (**Fig. 2B**). At 24 hpi, all cells were infected
189 and around 70% of them were positive for TIAR- and G3BP- containing foci. At 37 hpi, all cells
190 remained infected and around 20% of them exhibited TIAR- and G3BP positive foci. These foci

191 resembled the ones detected in Huh7 cells treated with sodium arsenite (NaArs), a chemical commonly
192 used for induction of oxidative stress in eukaryotic cells, for 30 minutes (**Fig. 2B**). These results indicate
193 that upon Asibi infection, TIAR- and G3BP- positive foci appeared between 12 and 15 hpi, peak around
194 24 hpi and persist in around 20% of cells until later times. Moreover, these data suggest that the
195 formation of the stress granules occur throughout infection with Asibi.

196 To further validate the nature of the TIAR- and G3BP- positive foci observed in infected cells, we
197 assessed their sensitivity to cycloheximide. Cycloheximide is a compound that inhibits stress granule
198 formation and fosters their disassembly by stabilizing mRNAs on polysomes (34). Huh7 cells treated
199 with NaArs for 30 min and subsequently incubated with cycloheximide for 1 hour or left untreated were
200 used as positive controls (**Fig. 2C**). Alternatively, cells were infected with Asibi for 48 hours and then
201 treated, or not, with cycloheximide for 1 hour. The TIAR and the G3BP signals overlapped, both in cells
202 infected by Asibi for 48 hours and in NaArs-treated cells (**Fig. 2C**). Cycloheximide treatment led to a
203 complete loss of TIAR- and G3BP- positive foci, both in NaArs-treated cells and in Asibi-infected cells
204 (**Fig. 2C**, compare non-treated and treated cells). These results suggest that, under both conditions, most
205 mRNAs trapped in these cytoplasmic foci can be released within 1 hour and undergo some translation
206 on polysomes. Most importantly, these experiments confirmed that the cytoplasmic foci containing
207 TIAR, G3BP and RIG-I identified in infected cells also contained mRNAs, and as such, can be defined
208 as canonical stress granules. Furthermore, these experiments also showed that the stress granule proteins
209 TIAR and G3BP are not recruited to Asibi replication complexes identified by NS4b, in contrast to
210 observations reported for ZIKV, DENV and WNV (35, 36).

211 We next monitored the formation of stress granules upon Asibi infection in different cell models
212 than Huh7. Like Huh7 cells, HepG2 cells are hepatocyte-derived cells and are thus relevant for infection
213 with YFV, a hepatotropic virus. TIAR- and G3BP-positive foci were detected in HepG2 cells infected
214 for 48 hours (**Fig. 3A**). Stress granules were also detected in CMMT cells, a *Macaca mulatta* epithelial
215 cell line, upon 24 hours of infection with Asibi (**Fig. 3B**). Macaques are natural hosts of YFV during
216 the jungle cycle of transmission (37). Similarly, TIAR- and G3BP-positive foci were observed in Huh7
217 cells infected with the clinical isolate HD1279 (HD Dakar) for 24 hours (**Fig. 3C**). These data indicate

218 that infection with two YFV strains triggers the formation of stress granules in several mammalian cell
219 lines, suggesting that the stress response is neither viral strain nor cell type specific.
220

221 **PKR contributes to stress granule formation and innate response in Asibi-infected Huh7 cells**

222 PKR is known to be activated upon infection with several flaviviruses, including ZIKV, WNV and
223 Japanese Encephalitis virus (JEV) (38–40) and to play an important role in stress granule nucleation
224 through its ability to phosphorylate the eukaryotic initiation factor eIF2α (41). We first assessed whether
225 PKR was activated upon Asibi infection of Huh7 cells. Western blot analysis showed that PKR was
226 phosphorylated in Huh7 cells infected for 24 and 48 hours, but not in non-infected cells (**Fig. 4A**). Thus,
227 PKR is activated upon Asibi infection of Huh7 cells. To evaluate the role of PKR in the formation of
228 stress granules in Asibi-infected human hepatic cells, we generated a Huh7 short hairpin (sh)-PKR cell
229 line by transduction with lentiviruses expressing short hairpin RNAs (shRNAs) specific for PKR. While
230 PKR expression was detectable in Huh7 cells transduced with lentivirus expressing control shRNA
231 targeting luciferase (Huh7-shLuc cells), it was not detectable in Huh7-shPKR cells (**Fig. 4B**). As a
232 control experiment, we treated the cells with NaArs, which induces stress granule formation *via* HRI-
233 mediated eIF2α phosphorylation (42). TIAR- and G3BP- positive stress granules were detected in both
234 Huh7-shLuc and Huh7-shPKR cells treated with NaArs for 30 minutes (**Fig. 4C**). This confirms that the
235 absence of PKR does not disrupt the formation of NaArs-dependent stress granule induction.

236 Automated microscopic quantification revealed that around 10% of Huh7-shLuc cells infected at a
237 MOI of 2 for 24 or 34 hours contained at least two stress granules (**Fig. 4 D-E**). At a MOI of 20, around
238 25% of Huh7-shLuc cells were positive for stress granules at 24 and 34 hpi (**Fig. 4 D-E)**. No TIAR- nor
239 G3BP- positive foci were detected in Huh7-shPKR cells infected at a MOI of 2 for 24 or 34 hours. At a
240 MOI of 20, a low percentage (around 1%) of Huh7-shPKR cells exhibited detectable stress granules
241 (**Fig. 4 D-E)**. These stress granules possibly formed in a PKR-independent manner, *via* the activation
242 of other members of the eIF2α kinase family. Alternatively, a minute quantity of PKR still being
243 expressed in shPKR cells may initiate the formation of these granules. A similar proportion of Huh7-
244 shLuc and Huh7-shPKR cells were found positive for NS4b at 24 or 34 hpi at the two tested MOIs (**Fig.**

245 **4F**). Together, we conclude that PKR plays a key role in stress granule formation in Asibi-infected
246 human hepatic cells and that the absence of stress granules has no effect on viral infection.
247 Since no stress granules were detected in cells depleted of PKR in three of four conditions tested
248 (**Fig. 4E**), we used Huh7-shPKR cells to determine whether absence of granules affected cytokine
249 induction. Consistent with our Western blot data (**Fig. 4B**), RT-qPCR analysis showed that *PKR* mRNAs
250 abundance was reduced by more than 90% in Huh7-shPKR cells in comparison to Huh7-shLuc cells
251 **(Fig. 5A**). (**Fig. 5B**), which is consistent with our microscopic analysis (**Fig. 4F**). *IL6* mRNA
252 abundance was significantly lower in Huh7-shPKR cells than that of Huh7-shLuc when cells were
253 infected at a MOI of 20 (**Fig. 5C).** The abundances of *TNFA* and *IFNB* mRNAs were significantly lower
254 in Huh7-shPKR cells than those in infected Huh7-shLuc under the same conditions of infection **(Fig.**
255 **5D-E**). This is consistent with our preceding observation of cytokine induction in Asibi infected cells
256 being dependent on NF-κB (**Fig. 1**) and with a previous report showing that PKR is involved in the
257 induction of the *IFN* through the activation of NF-κB (44). Thus, at least two nucleic acid sensors,
258 namely RIG-I (**Fig. 1**) and PKR (**Fig. 4** and **5**), contribute to the antiviral response against Asibi in Huh7
259 cells.
260 Taken together, our data show that PKR contributes to both stress granule formation and induction
261 of cytokines in Huh7 cells infected with Asibi. However, since PKR does not require its kinase activity
262 to stimulate NF-κB (44, 45), it might contribute to the cytokine induction in Asibi-infected cells in a
263 eIF2α- (and thus stress granule-) independent manner.
264
265 **Induction of pro-inflammatory cytokines is not affected by the inhibition of stress granules**
266 To further investigate the putative link between stress granules and the induction of antiviral
267 cytokines, we used a siRNA-knockdown approach to inhibit stress granule assembly. We tested
268 numerous combinations of siRNAs targeting core granule components in infected cells. The most
269 efficient strategy consisted in transfecting Huh7 cells twice with four pools of siRNAs targeting TIAR,
270 TIA-1, G3BP1 and G3BP2 (siSG). In these cells, we monitored stress granule formation using
271 antibodies against eIF3b and eIF4G, two core components of stress granules. Around 30% of Huh7 cells

272 transfected with scrambled control siRNAs and infected at a MOI of 2 or 20 for 24 hours contained at
273 least two eIF4G- and eIF3b-positive foci (**Fig. 6A-B**). When cells were transfected with the 4 siRNA
274 pools and infected under the same conditions and for the same amount of time, less than 5% of cells
275 exhibited stress granules (**Fig. 6A-B**). The impact of the siRNA against TIAR, TIA-1, G3BP1 and
276 G3BP2 on the number of cells positive for stress granules following 34 hours of infection was also
277 significant at the two tested MOIs (**Fig. 6B**). Under the four tested conditions, the surface area occupied
278 by stress granules per cell was significantly reduced in cells transfected with the mixture of four siRNA
279 pools compared to the controls (**Fig. 6C**). These experiments validate our silencing approach as an
280 efficient way to significantly reduce both the number of cells positive for stress granules and the surface
281 occupied by stress granules per cell. Transfection with the 4 siRNA pools had no effect on viral
282 infection, when compared to transfection with control siRNAs **(Fig. 6D**). RT-qPCR analysis showed
283 that TIAR, TIA-1, G3BP1 and G3BP2 mRNA abundances were significantly reduced in cells
284 transfected with the 4 siRNA pools as compared to cells transfected with control siRNAs **(Fig. 7A-D**).
285 Of note, TIAR and TIA-1 expression was induced three- to four-fold by infection, in an MOI-dependent
286 response. This may be a consequence of virally-induced stress. Transfection of the four siRNA pools
287 has no effect on *TNFA, IL6* and *IFNB* mRNA abundances nor on viral RNA yield **(Fig. 7E-H**). Together,
288 these data show that significant reduction of stress granule numbers and size did not suppress the
289 cytokine response to Asibi infection. Thus, in our model, stress granules do not contribute to the
290 initiation of the antiviral response.
291
292 **RIG-I signaling is not involved in stress granule assembly**
293 In Huh7 cells, RIG-I signaling is crucial for cytokine induction and secretion upon Asibi infection
294 (**Fig. 1**). Therefore, we wondered whether RIG-I signaling would participate in stress granule assembly
295 and/or maintenance. We quantified the proportion of Huh7 and Huh7.5 cells that were positive for stress
296 granules at 24 and 34 hpi following infection at two MOIs. A similar proportion of Huh7 and Huh7.5
297 cells were found positive for stress granule markers in all tested conditions (**Fig. 8 A-B**). No difference
298 in the number of cells positive for NS4b was observed between Huh7 and Huh7.5 cells (**Fig. 8C**). We
299 conclude that the absence of RIG-I signaling had no effect on the number of granules that assemble in

300 response to infection. It is thus unlikely that RIG-I mediates a feed-forward loop to maintain stress
301 granule assembly.
302
303 **YFV RNA is excluded from stress granules**
304 Our previous analysis showed that neither dsRNA (**Fig. 2A**) nor the viral proteins NS4b and NS1
305 (**Fig. 2B, 2C, 3, 4D, 6A** and **8A**) seem to be recruited to stress granules. To further investigate the
306 putative association between stress granules containing RIG-I (**Fig. 2A**) and viral RNA, we used an
307 RNA fluorescence *in situ* hybridization (FISH) approach coupled with immunofluorescence and
308 confocal microscopy. The Asibi-specific FISH probe produced no signal in non-infected Huh7 control
309 cells (**Fig. 9A**) and a bright punctate signal in the cytoplasm of infected cells (**Fig. 9A**), confirming the
310 specificity of the probe (46). Asibi RNA was never found to be associated with TIAR (**Fig. 9A**). This
311 was unexpected since RIG-I signaling is key to cytokine induction and production (**Fig. 1**) and massively
312 concentrate in stress granules in Asibi-infected cells (**Fig. 2A**). These results suggest that an interaction
313 between viral RNA and RIG-I might not happen in stress granules in Asibi-infected Huh7 cells. A
314 minute quantity of RIG-I might however interact with viral RNA in ER-derived replication sites and
315 initiates a stress granule-independent IFN response. In line with this, RIG-I was recruited to TIAR-
316 positive granules in Huh7 cells treated with NaArs (**Fig. 9B**), which is consistent with previous
317 observations on NaArs-treated HeLa cells (20). These data further indicate that RIG-I recruitment to
318 stress granules can occur in absence of viral RNA.
319
320 **Discussion**
321 The identity of the PRR(s) responsible for the initiation of a pro-inflammatory response upon direct
322 infection of human hepatocytes with wild-type strains of YFV has not been uncovered thus far. In this
323 study, we first identified RIG-I and PKR as main actors responsible for the induction and production of
324 pro-inflammatory cytokines upon infection of human hepatocytes with the Asibi strain of YFV. We
325 demonstrated the crucial involvement of RIG-I in this process by directly comparing the dysfunctional
326 RIG-I-expressing human hepatoma cell line Huh7.5. with its RIG-I -competent counterpart (Huh7 cells).

327 The level of IL6 and TNFα secreted in the first 48 hours of infection by Huh7.5 cells upon Asibi
328 infection was under the limit of detection, whilst both cytokines were produced in Huh7 cells in the
329 same experimental conditions. This is in accordance with our previous studies showing that human
330 plasmacytoid dendritic cells infected with the YFV vaccine strain 17D induced an IFN response in a
331 RIG-I dependent manner (19). Other members of the RLR family may contribute to YFV sensing in
332 other cell types or at later time of infection. Such distinct temporal activity of RIG-I and MDA5 during
333 infection with the related West Nile Virus has been reported in mice (47).

334 In Huh7 cells silenced for PKR and infected with Asibi, cytokine expression was, in most of the
335 tested conditions, below the detection limit. This suggests that PKR, like RIG-I, largely contributes to
336 the initiation of the antiviral response. This is consistent with the previously reported role of PKR in the
337 production of IFN and other pro-inflammatory cytokines upon viral infection, possibly *via* its interaction
338 with the IKK complex and subsequent activation of NF-κB (44, 48). Moreover, PKR was previously
339 described as an important effector protein against infection with WNV in mice (40).

340 The fact that abolishing RIG-I signaling or silencing PKR drastically reduces the pro-inflammatory
341 response in Asibi infected cells shows the non-redundant nature of these two dsRNA sensors in
342 maintaining cytokine production. We speculate that RIG-I and PKR cooperate to induce an anti-YFV
343 response. Indeed, PKR interacts with RIG-I and MDA5 in HEK293T cells transfected with FLAG-
344 tagged versions of RIG-I or MDA5 and infected with a mutant vaccinia virus lacking a gene known to
345 inhibit PKR (49). However, in this context, PKR was only required for MDA5, but not RIG-I mediated,
346 IFN production (49). Consistent with the hypothesis that PKR and RIG-I cooperate to orchestrate
347 antiviral response, PKR is known to interact with several members of the TRAF family, including
348 TRAF2 and TRAF6 (50, 51), two proteins involved in MAVS signaling. Finally, MAVS, which acts
349 downstream of RIG-I and MDA5, interacts with PKR (52) and is essential for PKR-induced IFN
350 production (49).

351 Stress granules have been demonstrated to contain and concentrate viral nucleic sensors; hence,
352 they are generally regarded as a functional platform for ligand recognition and subsequent induction of
353 an antiviral response. We report here that Asibi replication triggers the formation of stress granules in
354 human hepatoma cells and epithelial monkey cells. This is consistent with previous studies showing that

355 infection with the vaccine strain 17D induces the formation of stress granules in human dendritic cells
356 and hamster kidney cells (53). Thus, formation of stress granules seems to be a general feature of
357 flavivirus infection (35, 36, 54, 55). However, unlike WNV, DENV, ZIKV and the related tick-borne
358 encephalitis virus (35, 36, 38, 54–57), YFV does not seem to efficiently antagonize stress granule
359 biogenesis. YFV may not express proteins that inhibit granule formation. Alternatively, stress granules
360 may not have an antiviral function against YFV and thus the virus has no pressure to evolve an evasion
361 strategy.

362 Stress granules were not detected in Huh7 cells depleted of PKR upon 24 hours of Asibi infection,
363 strongly suggesting a PKR-dependent granule establishment early in infection. Of note, RIG-I signaling
364 was not involved in stress granule assembly, indicating that, whilst the two sensors are both critically
365 implicated in the pro-inflammatory cytokine production, only PKR is able to activate stress granule
366 formation. At 34 hours, very few cells silenced for PKR exhibited stress granules. Small quantities of
367 remaining PKR, below the detection limit of Western blot and qPCR analysis, may be responsible for
368 the formation of these foci. Alternatively, they may form subsequent to the phosphorylation of eIF2α
369 by one of the other three eIF2α kinases. YFV replication and assembly, which takes place within ER
370 membranes (3), likely causes an ER stress and might thus trigger the activation of the ER resident kinase
371 PERK. Since GCN2 is phosphorylated in mouse and human dendritic cells upon infection with 17D
372 (53), this kinase could also potentially contribute to granule formation in Asibi infected cells.

373 Similar to what was reported in the context of infection with numerous RNA viruses (27, 28, 58),
374 we showed that RIG-I accumulates in stress granules upon Asibi infection. PKR, MDA5, LGP2 and the
375 DNA sensor cGAS were also shown to concentrate in stress granules in cells infected with a large panel
376 of RNA and DNA viruses (20, 22–26). However, we were unable to detect neither Asibi RNA nor
377 dsRNA structures in stress granules of infected cells. Thus, the interaction between YFV RNA by RIG-
378 I and PKR is unlikely to occur in stress granules. Similarly, in cells infected with Orthohantaviruses, no
379 viral RNA was found associated with stress granules (59). Conversely, viral RNA was detected in stress
380 granules induced by infection with IAVΔNS1 (20). We propose that, at least in Asibi-infected cells, the
381 large accumulation of PKR and RIG-I in stress granules masks the detection of small quantities of PKR
382 and RIG-I which are recruited to perinuclear ER-derived replication sites, where viral RNA sensing may

383 occur. Importantly, inhibition of stress granule formation didn't affect the pro-inflammatory cytokine
384 expression by infected hepatocytes, indicating that the anti-viral response and stress granules formation
385 are independent events in the early phases of YFV infection. Whether the formation of stress granules
386 and their composition affect later stages of infection remains to be established.

387 Collectively, our data strongly suggest that, in cells infected with YFV, pro-inflammatory cytokine
388 induction is mediated by RIG-I and PKR, independent of their localization in stress granules. Thus,
389 contrary to the widely believed consensus, we demonstrated that the stress granule formation can be
390 uncoupled from the initiation of a pro-inflammatory response upon viral infection.

391

392

393 **Materials and Methods**

394 **Cell lines, virus, antibodies and reagents**

395 Huh7 human hepatocellular carcinoma cells (kindly provided by A. Martin, Institut Pasteur Paris)
396 and Huh7.5 cells (60) were maintained in Dulbecco's modified eagle's medium (DMEM)(Gibco)
397 containing GlutaMAX I and sodium pyruvate (Invitrogen) supplemented with 10% heat-inactivated
398 foetal bovine serum (FBS, Dominique Dutscher) and 1% penicillin and streptomycin (P/S, 10.000 U/ml,
399 Thermofischer). HepG2 cells (kindly provided by C. Neuveut, Institut Pasteur Paris) were maintained
400 in DMEM-F12 complemented with 10% FBS, 3.5×10^{-7} M hydrocortisone, and 5 µg/ml insulin. Human
401 embryonic kidney (HEK) 293FT cells (American Type Culture Collection; ATCC CRL-1573), *Macaca*
402 *mulatta* mammary gland epithelial CMMT cells (kindly provided by O. Schwartz, Institut Pasteur Paris)
403 and African green monkey kidney epithelial Vero cells (ATCC) were maintained in DMEM 10% FBS.

404 The Asibi strain, which is the YFV reference strain was provided by the Biological Resource Center
405 of Institut Pasteur. The YFV-DAK strain (YFV-Dakar HD1279) was provided by the World Reference
406 Center for Emerging Viruses and Arboviruses (WRCEVA), through the University of Texas Medical
407 Branch at Galveston, USA. Virus stocks were propagated on Vero cells. Viruses were concentrated by
408 polyethylene glycol 6000 precipitation and purified by centrifugation in a discontinued gradient of
409 sucrose. Infectious virus titers were determined by plaque assays on Vero cells. Cells were infected
410 with 10-fold serial dilutions of viral stocks and incubated for 4 days in DMEM containing 2% FBS and

411 carboxymethyl cellulose. Cells were then washed with PBS, fixed with 3% formaldehyde crystal violet
412 solution for 20 min at room temperature, rinsed with water and plaques were counted. Cell infections
413 were carried out at the indicated MOIs. The viral inoculum was replaced with fresh culture medium two
414 hours post-infection.

415 The following antibodies were used: pIRF3 S386 (clone EPR2346, Abcam), IRF3 (FL-425, Santa
416 Cruz), NF-κB p65 (D14E12, Cell Signalling), IκBα (L35A5, Cell Signalling), β-Actin (clone AC-74,
417 Sigma-Aldrich), dsRNA J2 (English & Scientific Consulting Kft), G3BP (BD Biosciences), TIAR (C-
418 18, Santa-Cruz), eIF4G (sc-11373, Santa-Cruz), eIF3b (N-20, sc-16377), YFV-NS4b (kind gift from
419 C.M. Rice, Rockefeller University), Alexa Fluor® 488 donkey Anti-Goat IgG (H+L), Alexa Fluor®
420 594 donkey Anti-Mouse IgG (H+L), Alexa Fluor® 647 donkey Anti-Rabbit IgG (H+L) (Life
421 Technologies), anti-mouse 680 (LI-COR Bioscience), anti-rabbit 800 (Thermo Fisher Scientific). The
422 RIG-I antibody was previously described (20).

423 Sodium arsenite (NaArs, Sigma) and Cycloheximide (CHX, Sigma) were diluted in water and used
424 at the indicated concentration.

425

426 **Generation of shRNA-expressing Huh7 cells by lentiviral transduction**

427 pALPS-shPKR1 and pALPS-shPKR3 were generated by cloning the following sequences in
428 pALPS (61): (TGC TGT TGA CAG TGA GCG CCA GCA GAT ACA TCA GAG ATA ATA GTG
429 AAG CCA CAG ATG TAT TAT CTC TGA TGT ATC TGC TGA TGC CTA CTG CCT CGG A) and
430 (TGC TGT TGA CAG TGA GCG ACA GAA GAA AAG ACT AAC TGT ATA GTG AAG CCA CAG
431 ATG TAT ACA GTT AGT CTT TTC TTC TGG TGC CTA CTG CCT CGG A). HEK293FT cells were
432 transfected with pCMV-VSV-G codon-optimized, pCMVR8.74 (both plasmids were given by P.
433 Charneau, Institut Pasteur) and lentiviral vectors (pALPS-shPKR1/3 or pALPS-shLuc) at a mass ratio
434 of 1:4:4. Huh7 cells were transduced with supernatant from transfected HEK293FT and selected with
435 10 μg/μL puromycin (Sigma Aldrich) four days later.

436

437 **Small Interfering RNA (siRNA) transfection**

438 Huh7 cells were transfected using Lipofectamine RNAiMax (Life Technologies) at 30 nM final of
439 nontargeting scrambled negative control (siScr) or G3BP1, G3BP2 and TIAR siRNAs. Alternatively,
440 cells were transfected at 40 nM final of siRNA-TIA1. All siRNAs were obtained from Dharmacon (ON-
441 TARGETplus SMARTpool). Transfected cells were harvested or used for infection assays 48 hours
442 after transfection.
443
444 **Enzyme-linked immunosorbent assay (ELISA)**
445 The amount of TNFα and IL6 in cell-culture supernatants was quantified by ELISA using the Human
446 TNFα or IL6 ELISA kit (eBiosciences), according to manufacturer's instructions. The detection limits
447 were 4 pg/ml for TNFα and 2 pg/ml for IL6.
448
449 **Western blot analysis**
450 Cells were lysed in radioimmunoprecipitation assay (RIPA) buffer (Sigma) containing a protease and
451 phosphatase inhibitor mixture (Roche). Cell lysates were normalized for protein content, boiled in
452 NuPAGE LDS sample buffer (Thermo Fisher Scientific) in non-reducing conditions and the proteins
453 were separated by SDS-PAGE (NuPAGE 4-12% Bis-Tris Gel, Life Technologies). Proteins were
454 transferred to nitrocellulose membranes (Bio-Rad) using a Trans-Blot Turbo Transfer system (Bio-Rad).
455 After blocking with PBS-Tween-20 0,1% (PBST) containing 5% milk or BSA for 1 hour at RT, the
456 membrane was incubated overnight at 4 °C with primary antibodies diluted in a blocking buffer. Finally,
457 the membrane was incubated for 45 min at RT with secondary antibodies (Anti-rabbit/mouse IgG (H+L)
458 DyLight 680/800) diluted in a blocking buffer, washed, and scanned using an Odyssey CLx infrared
459 imaging system (LI-COR Bioscience).
460
461 **RNA extraction and RT-qPCR analysis**
462 Total RNAs were extracted from cell-lysates using the NucleoSpin RNA II Kit (Macherey-Nagel)
463 following the manufacturer's protocol and were eluted in nuclease-free water. First-strand
464 complementary DNA synthesis was performed with the RevertAid H Minus M-MuLV Reverse
465 Transcriptase (Thermo Fisher Scientific). Quantitative real-time PCR was performed on a real-time PCR

466 system (QuantStudio 6 Flex, Applied Biosystems) with SYBR Green PCR Master Mix (Life
467 Technologies). Data were analyzed with the ΔΔCT method, with all samples normalized to GAPDH.
468 All experiments were performed in technical triplicate. Primers used in this study are: GAPDH (GGT
469 CGG AG TCA ACG GAT TTG and ACT CCA CGA CGT ACT CAG CG), YF-NS3 (GCG TAA GGC
470 TGG AAA GAG TG and CTT CCT CCC TTC ATC CAC AA), TNFA (GCC CAT GTT GTA GCA
471 AAC CC and GGA GGT TGA CCT TGG TCT GG), IL6 (TGC AAT AAC CAC CCC TGA CC and
472 GTG CCC ATG CTA CAT TTG CC), IFNB (AAG CAA TTG TCC AGT CCC A and TGC ATT ACC
473 TGA AGG CCA AG), PKR (CAG AAT TGA CGG AAA GAC TTA CG and CTC TCA AGA GAA
474 TCA TCA CTG GT), G3BP1 (CAG TTA TAT AGA CCG GCG GC and TAT GTC CAA ACC TAC
475 GCG GC), G3BP2 (CAA TCT CAG CCA CCT CGT GT and CCA CAA CGT TTC CAA AAC TCA
476 T), TIAR (CGT CTG GGT TAA CAG ATC AGC and CAT GGG CTG CAC TTT CAT GG), TIA1
477 (AAT CCC GTG CAA CAG CAG GA and AGG CGG TTG CAC TCC ATA AT). Viral genome
478 equivalents concentrations (GE/ml) were determined by extrapolation from a standard curve generated
479 from serial dilutions of the plasmid encoding the YF-R.luc2A-RP (62).
480
481 **Immunofluorescence, fluorescence *in situ* hybridization (FISH) and confocal analysis.**
482 Cells were fixed with 4% paraformaldehyde (PFA; Sigma-Aldrich) for 30 min at RT, permeabilized
483 with 0.5% Triton X-100 in PBS and then blocked with 0,05% Tween-, 5% BSA-containing PBS before
484 incubation with the indicated primary antibodies. Antibody labelling was revealed with Alexa Fluor®
485 488-, 594 or 647-conjugated antibodies. Coverslips were mounted on slides using ProLong® Gold
486 Antifade Reagent with NucBlue solution (Invitrogen). Images were acquired with a Zeiss LSM 700
487 inverted confocal microscope. Fluorescence in situ hybridization was performed after immunostaining.
488 The (+) RNA strands of YFV were detected following the manufacturer's protocol (ViewRNA ISH
489 Cells Assays) using probe sets designed by Affymetrix. The Alexa-Fluor 546-conjugated (+)-strand
490 probe set targets a region between position nucleotides 4567 and 5539 of the YFV genome. Intensity
491 plot data were generated using Zen 2 lite (Zeiss) and plotted using GraphPad Prism 6.
492
493 **Stress granule quantification**

494 Nucleus and stress granule quantifications were performed using CellProfiler (v3.0.0) using custom
495 pipeline (available on request). In a nutshell: (i) nuclei were detected using the NucBlue signal, (ii)
496 cellular border were estimated using TIAR or eiF3b signal, (iii) stress granule borders were estimated
497 using G3BP, TIAR, eIF4G or eIF3b signals. Further analyses were performed using R and R studio (63).
498 Cells were considered positive for stress granules if they exhibited at least two of them.
499

500 **Statistical analysis**

501 Data are presented as means ± SD and were analyzed using GraphPad Prism 6. Statistical analysis of
502 percentage values or fold enrichment values were performed on logit or log-transformed values,
503 respectively. Statistical analysis was performed with two tailed unpaired t-test with Welch correction
504 for pairwise comparisons or by one- or two-way analysis of variance (ANOVA) with Tukey's or
505 Dunnet's multiple comparisons test when comparing more than two sets of values. Each experiment was
506 performed at least twice, unless otherwise stated. Statistically significant differences are indicated as
507 follows: *: $p < 0.05$, **: $p < 0.01$ and ***: $p < 0.001$; ns, not significant.
508

509 **Acknowledgments**. We thank Charlie Rice for generously providing the anti-YFV-NS4b antibodies;
510 Richard Kuhn for the YFV replicon construct, Marie Flamand for anti-NS1 antibodies (17A12),
511 Christine Neuveut for the HepG2 cells, Olivier Schwartz for the CMMT cells, Annette Martin for Huh7
512 cells, Pamela Schnupf for eIF3b and eIF4G antibodies, Pierre Charneau for the plasmids pCMV-VSV-
513 G and pCMVR8.74, Andrea Cimarelli for the pALPS plasmid, Olivier Disson for immuno-
514 histochemistry advice and Léa Richard for cloning shPKR into pALPS. We are grateful to the members
515 of our laboratory for helpful discussions and technical advice. We thank Audrey Salles and Julien
516 Fernandes (UTechS Photonic Bioimaging platform, Institut Pasteur) for their help in confocal
517 acquisition. We are grateful to Stéphane Rigaud (Image Analysis Hub, Institut Pasteur) for his advice
518 in analyzing confocal images and to Vincent Guillemot (Bioinformatics and Biostatistics HUB, Institut
519 Pasteur) for his help in statistical analysis. Finally, we thank Stephanie Straubel for critical reading of
520 the manuscript.

521

522 **References**

523 1. Gould EA, Solomon T. 2008. Pathogenic flaviviruses. Lancet 371:500–9.
524 2. Gubler DJ, Kuno G, Markoff L. 2007. Flaviviruses, p. 1153–1252. *In* Fields
525 Virology5th Edition.
526 3. Douam F, Ploss A. 2018. Yellow Fever Virus: Knowledge Gaps Impeding the Fight
527 Against an Old Foe. Trends Microbiol 26:913–928.
528 4. Pulendran B. 2009. Learning immunology from the yellow fever vaccine: innate
529 immunity to systems vaccinology. Nat Rev Immunol 9:741–7.
530 5. Barrett AD. 2016. Yellow Fever in Angola and Beyond--The Problem of Vaccine
531 Supply and Demand. N Engl J Med 375:301–3.
532 6. Barrett ADT. 2018. The reemergence of yellow fever. Science 361:847–848.
533 7. Messaoudi I, Basler CF. 2015. Immunological features underlying viral hemorrhagic
534 fevers. Curr Opin Immunol 36:38–46.
535 8. Paessler S, Walker DH. 2013. Pathogenesis of the viral hemorrhagic fevers. Annu Rev
536 Pathol 8:411–40.
537 9. Chen IY, Ichinohe T. 2015. Response of host inflammasomes to viral infection.
538 Trends Microbiol 23:55–63.
539 10. ter Meulen J, Sakho M, Koulemou K, Magassouba N, Bah A, Preiser W, Daffis S,
540 Klewitz C, Bae HG, Niedrig M, Zeller H, Heinzel-Gutenbrunner M, Koivogui L, Kaufmann
541 A. 2004. Activation of the cytokine network and unfavorable outcome in patients with yellow
542 fever. The Journal of infectious diseases 190:1821–7.
543 11. Engelmann F, Josset L, Girke T, Park B, Barron A, Dewane J, Hammarlund E, Lewis
544 A, Axthelm MK, Slifka MK, Messaoudi I. 2014. Pathophysiologic and transcriptomic
545 analyses of viscerotropic yellow fever in a rhesus macaque model. PLoS Negl Trop Dis
546 8:e3295.
547 12. Streicher F, Jouvenet N. 2019. Stimulation of Innate Immunity by Host and Viral
548 RNAs. Trends in Immunology 40:1134–1148.
549 13. Chow KT, Gale M, Loo Y-M. 2018. RIG-I and Other RNA Sensors in Antiviral
550 Immunity. Annual Review of Immunology 36:667–694.
551 14. Nan Y, Nan G, Zhang YJ. 2014. Interferon induction by RNA viruses and antagonism
552 by viral pathogens. Viruses 6:4999–5027.
553 15. Chazal M, Beauclair G, Gracias S, Najburg V, Simon-Loriere E, Tangy F, Komarova
554 AV, Jouvenet N. 2018. RIG-I Recognizes the 5' Region of Dengue and Zika Virus Genomes.
555 Cell Rep 24:320–328.
556 16. Sprokholt JK, Kaptein TM, van Hamme JL, Overmars RJ, Gringhuis SI, Geijtenbeek
557 TBH. 2017. RIG-I-like Receptor Triggering by Dengue Virus Drives Dendritic Cell Immune
558 Activation and TH1 Differentiation. J Immunol 198:4764–4771.
559 17. Sprokholt JK, Kaptein TM, van Hamme JL, Overmars RJ, Gringhuis SI, Geijtenbeek
560 TBH. 2017. RIG-I-like receptor activation by dengue virus drives follicular T helper cell
561 formation and antibody production. PLoS Pathog 13:e1006738.
562 18. Hertzog J, Junior AGD, Rigby RE, Donald CL, Mayer A, Sezgin E, Song C, Jin B,
563 Hublitz P, Eggeling C, Kohl A, Rehwinkel J. 2018. Infection with a Brazilian isolate of Zika
564 virus generates RIG-I stimulatory RNA and the viral NS5 protein blocks type I IFN induction
565 and signaling. European Journal of Immunology 48:1120–1136.
566 19. Bruni D, Chazal M, Sinigaglia L, Chauveau L, Schwartz O, Despres P, Jouvenet N.
567 2015. Viral entry route determines how human plasmacytoid dendritic cells produce type I
568 interferons. Sci Signal 8:ra25.
569 20. Onomoto K, Jogi M, Yoo J-S, Narita R, Morimoto S, Takemura A, Sambhara S,

570 Kawaguchi A, Osari S, Nagata K, Matsumiya T, Namiki H, Yoneyama M, Fujita T. 2012.
571 Critical Role of an Antiviral Stress Granule Containing RIG-I and PKR in Viral Detection and
572 Innate Immunity. PLOS ONE 7:e43031.
573 21. Oh S-W, Onomoto K, Wakimoto M, Onoguchi K, Ishidate F, Fujiwara T, Yoneyama
574 M, Kato H, Fujita T. 2016. Leader-Containing Uncapped Viral Transcript Activates RIG-I in
575 Antiviral Stress Granules. PLOS Pathogens 12:e1005444.
576 22. Yoo J-S, Takahasi K, Ng CS, Ouda R, Onomoto K, Yoneyama M, Lai JC, Lattmann
577 S, Nagamine Y, Matsui T, Iwabuchi K, Kato H, Fujita T. 2014. DHX36 enhances RIG-I
578 signaling by facilitating PKR-mediated antiviral stress granule formation. PLoS Pathog
579 10:e1004012.
580 23. Sánchez-Aparicio MT, Ayllón J, Leo-Macias A, Wolff T, García-Sastre A. 2017.
581 Subcellular Localizations of RIG-I, TRIM25, and MAVS Complexes. J Virol 91.
582 24. Langereis MA, Feng Q, Kuppeveld FJ van. 2013. MDA5 Localizes to Stress Granules,
583 but This Localization Is Not Required for the Induction of Type I Interferon. Journal of
584 Virology 87:6314–6325.
585 25. Narita R, Takahasi K, Murakami E, Hirano E, Yamamoto SP, Yoneyama M, Kato H,
586 Fujita T. 2014. A Novel Function of Human Pumilio Proteins in Cytoplasmic Sensing of
587 Viral Infection. PLOS Pathogens 10:e1004417.
588 26. Hu S, Sun H, Yin L, Li J, Mei S, Xu F, Wu C, Liu X, Zhao F, Zhang D, Huang Y, Ren
589 L, Cen S, Wang J, Liang C, Guo F. 2019. PKR-dependent cytosolic cGAS foci are necessary
590 for intracellular DNA sensing. Sci Signal 12.
591 27. Onomoto K, Yoneyama M, Fung G, Kato H, Fujita T. 2014. Antiviral innate immunity
592 and stress granule responses. Trends Immunol 35:420–428.
593 28. McCormick C, Khaperskyy DA. 2017. Translation inhibition and stress granules in the
594 antiviral immune response. Nat Rev Immunol 17:647–660.
595 29. Ivanov P, Kedersha N, Anderson P. 2019. Stress Granules and Processing Bodies in
596 Translational Control. Cold Spring Harb Perspect Biol 11:a032813.
597 30. Reineke LC, Lloyd RE. 2013. Diversion of stress granules and P-bodies during viral
598 infection. Virology 436:255–267.
599 31. Sumpter R, Loo YM, Foy E, Li K, Yoneyama M, Fujita T, Lemon SM, Gale M. 2005.
600 Regulating intracellular antiviral defense and permissiveness to hepatitis C virus RNA
601 replication through a cellular RNA helicase, RIG-I. J Virol 79:2689–99.
602 32. Kedersha N, Cho MR, Li W, Yacono PW, Chen S, Gilks N, Golan DE, Anderson P.
603 2000. Dynamic Shuttling of Tia-1 Accompanies the Recruitment of mRNA to Mammalian
604 Stress Granules. J Cell Biol 151:1257–1268.
605 33. Bonenfant G, Williams N, Netzband R, Schwarz MC, Evans MJ, Pager CT. 2019.
606 Zika Virus Subverts Stress Granules To Promote and Restrict Viral Gene Expression. Journal
607 of Virology 93.
608 34. Emara MM, Brinton MA. 2007. Interaction of TIA-1/TIAR with West Nile and
609 dengue virus products in infected cells interferes with stress granule formation and processing
610 body assembly. Proceedings of the National Academy of Sciences 104:9041–9046.
611 35. Monath TP. 2005. Yellow fever vaccine. Expert review of vaccines 4:553–74.
612 36. Hou S, Kumar A, Xu Z, Airo AM, Stryapunina I, Wong CP, Branton W, Tchesnokov
613 E, Götte M, Power C, Hobman TC. 2017. Zika Virus Hijacks Stress Granule Proteins and
614 Modulates the Host Stress Response. Journal of Virology 91.
615 37. Tu Y-C, Yu C-Y, Liang J-J, Lin E, Liao C-L, Lin Y-L. 2012. Blocking Double-
616 Stranded RNA-Activated Protein Kinase PKR by Japanese Encephalitis Virus Nonstructural
617 Protein 2A. Journal of Virology 86:10347–10358.
618 38. Samuel MA, Whitby K, Keller BC, Marri A, Barchet W, Williams BRG, Silverman
619 RH, Gale M, Diamond MS. 2006. PKR and RNase L Contribute to Protection against Lethal

620 West Nile Virus Infection by Controlling Early Viral Spread in the Periphery and Replication
621 in Neurons. J Virol 80:7009–7019.
622 39. Dabo S, Meurs EF. 2012. dsRNA-Dependent Protein Kinase PKR and its Role in
623 Stress, Signaling and HCV Infection. Viruses 4:2598–2635.
624 40. Lu L, Han AP, Chen JJ. 2001. Translation initiation control by heme-regulated
625 eukaryotic initiation factor 2alpha kinase in erythroid cells under cytoplasmic stresses. Mol
626 Cell Biol 21:7971–7980.
627 41. Bonnet MC, Weil R, Dam E, Hovanessian AG, Meurs EF. 2000. PKR stimulates NF-
628 kappaB irrespective of its kinase function by interacting with the IkappaB kinase complex.
629 Mol Cell Biol 20:4532–4542.
630 42. Bonnet MC, Daurat C, Ottone C, Meurs EF. 2006. The N-terminus of PKR is
631 responsible for the activation of the NF-κB signaling pathway by interacting with the IKK
632 complex. Cellular Signalling 18:1865–1875.
633 43. Sinigaglia L, Gracias S, Decembre E, Fritz M, Bruni D, Smith N, Herbeuval JP,
634 Martin A, Dreux M, Tangy F, Jouvenet N. 2018. Immature particles and capsid-free viral
635 RNA produced by Yellow fever virus-infected cells stimulate plasmacytoid dendritic cells to
636 secrete interferons. Sci Rep 8:10889.
637 44. Errett JS, Suthar MS, McMillan A, Diamond MS, Gale M. 2013. The essential,
638 nonredundant roles of RIG-I and MDA5 in detecting and controlling West Nile virus
639 infection. J Virol 87:11416–25.
640 45. Zamanian-Daryoush M, Mogensen TH, DiDonato JA, Williams BR. 2000. NF-
641 kappaB activation by double-stranded-RNA-activated protein kinase (PKR) is mediated
642 through NF-kappaB-inducing kinase and IkappaB kinase. Mol Cell Biol 20:1278–1290.
643 46. Pham AM, Santa Maria FG, Lahiri T, Friedman E, Marié IJ, Levy DE. 2016. PKR
644 Transduces MDA5-Dependent Signals for Type I IFN Induction. PLoS Pathog 12.
645 47. Gil J, García MA, Gomez-Puertas P, Guerra S, Rullas J, Nakano H, Alcamí J, Esteban
646 M. 2004. TRAF Family Proteins Link PKR with NF-κB Activation. Molecular and Cellular
647 Biology 24:4502–4512.
648 48. Arnaud N, Dabo S, Akazawa D, Fukasawa M, Shinkai-Ouchi F, Hugon J, Wakita T,
649 Meurs EF. 2011. Hepatitis C virus reveals a novel early control in acute immune response.
650 PLoS Pathog 7:e1002289.
651 49. Zhang P, Li Y, Xia J, He J, Pu J, Xie J, Wu S, Feng L, Huang X, Zhang P. 2014. IPS-1
652 plays an essential role in dsRNA-induced stress granule formation by interacting with PKR
653 and promoting its activation. J Cell Sci 127:2471–2482.
654 50. Ravindran R, Khan N, Nakaya HI, Li S, Loebbermann J, Maddur MS, Park Y, Jones
655 DP, Chappert P, Davoust J, Weiss DS, Virgin HW, Ron D, Pulendran B. 2014. Vaccine
656 activation of the nutrient sensor GCN2 in dendritic cells enhances antigen presentation.
657 Science 343:313–317.
658 51. Albornoz A, Carletti T, Corazza G, Marcello A. 2014. The stress granule component
659 TIA-1 binds tick-borne encephalitis virus RNA and is recruited to perinuclear sites of viral
660 replication to inhibit viral translation. J Virol 88:6611–6622.
661 52. Roth H, Magg V, Uch F, Mutz P, Klein P, Haneke K, Lohmann V, Bartenschlager R,
662 Fackler OT, Locker N, Stoecklin G, Ruggieri A. 2017. Flavivirus Infection Uncouples
663 Translation Suppression from Cellular Stress Responses. mBio 8.
664 53. Basu M, Courtney SC, Brinton MA. 2017. Arsenite-induced stress granule formation
665 is inhibited by elevated levels of reduced glutathione in West Nile virus-infected cells. PLOS
666 Pathogens 13:e1006240.
667 54. Amorim R, Temzi A, Griffin BD, Mouland AJ. 2017. Zika virus inhibits eIF2α-
668 dependent stress granule assembly. PLOS Neglected Tropical Diseases 11:e0005775.
669 55. Zhang Q, Sharma NR, Zheng Z-M, Chen M. 2019. Viral Regulation of RNA Granules

670 in Infected Cells. Virol Sin 34:175–191.
671 56. Christ W, Tynell J, Klingström J. 2020. Puumala and Andes Orthohantaviruses Cause
672 Transient Protein Kinase R-Dependent Formation of Stress Granules. J Virol 94.
673 57. Blight KJ, McKeating JA, Rice CM. 2002. Highly permissive cell lines for
674 subgenomic and genomic hepatitis C virus RNA replication. J Virol 76:13001–14.
675 58. Pertel T, Hausmann S, Morger D, Zuger S, Guerra J, Lascano J, Reinhard C, Santoni
676 FA, Uchil PD, Chatel L, Bisiaux A, Albert ML, Strambio-De-Castillia C, Mothes W, Pizzato
677 M, Grutter MG, Luban J. 2011. TRIM5 is an innate immune sensor for the retrovirus capsid
678 lattice. Nature 472:361–5.
679 59. Jones CT, Patkar CG, Kuhn RJ. 2005. Construction and applications of yellow fever
680 virus replicons. Virology 331:247–59.
681 60. RStudio Team. 2016. RStudio: Integrated Development Environment for R.
682

683

684

685 **Figure legends**

686

687 **Fig. 1: The Asibi strain of YFV triggers the production of pro-inflammatory cytokines in**
688 **hepatoma cells through RIG-I, IRF3 and NF-κB**

689 Huh7 and Huh7.5 cells were left uninfected or infected with Asibi at an MOI of 1 for 24 or 48 hours.
690 The relative amounts of *IL6* (**A**), *TNFA* (**B**) and *IFNB* (**C**) mRNAs were determined by RT-qPCR
691 analysis and normalized to GAPDH mRNA and non-infected samples. The relative amounts of cell-
692 associated viral RNA were determined by RT-qPCR analysis (**D**) and expressed as genome equivalents
693 (YFV-GE) per µg of total cellular RNA. The data are the means ± SD of two (Huh7.5) or three (Huh7)
694 independent experiments. ns: non-significant, *: $p<0.05$, **: $p<0.01$. (**E**, **F**) Culture media of the
695 indicated cells were analysed by ELISA to determine the amounts of secreted IL6 (**E**) and TNFα (**F**).
696 The data are the means ± SD of two (Huh7.5) or three (Huh7). The dashed lines indicate the limit of
697 detection of the IL6 and TNFα ELISA (2 and 4 pg/ml, respectively). (**G**) Whole-cell lysates of the
698 indicated cells were analysed by Western blotting with antibodies against the indicated proteins. (**H**, **I**)
699 Huh7 cells were left uninfected (NI) or infected with YFV-Asibi for 48 hours at an MOI of 20. Cells
700 were then stained with IRF3 (**H**) or p65 (**I**) (red), dsRNA (green) antibodies and NucBlue® (blue).
701 Around 200 cells per independent experiment were scored for nuclear translocation of IRF3 or p65 (**H**
702 and **I**, respectively). ns: non-significant, *: $p<0.05$.

703

704 **Fig. 2: RIG-I localizes to stress granules in Huh7 cells infected with YFV**

705 (**A**) Huh7 cells were left uninfected (NI) or infected with Asibi at MOI of 20 for 24 hours. Cells were
706 then stained with dsRNA (red), RIG-I (purple), TIAR (green) antibodies and NucBlue® (blue). (**B**)
707 Huh7 cells were left uninfected (NI), treated with 0.5 mM NaArs for 30 min or infected with Asibi at
708 an MOI of 20 for the indicated time. Cells were then stained with NS4b (purple), G3BP (red), TIAR
709 (green) antibodies and NucBlue® (blue). Percentage of NS4b-positive and G3BP-positive cells were
710 estimated and shown in purple and yellow respectively. (**C**) Huh7 cells were treated with 0.5 mM NaArs
711 for 30 min or infected with YFV-Asibi at MOI of 20 for 48 hours. Cells were then left untreated (NT)

712 or treated with 100 µg/mL Cycloheximide (CHX) for 1 hour and stained with antibodies against NS4b
713 (purple), TIAR (green) and G3BP (red), as well as with NucBlue® (blue).
714
715 **Fig. 3: YFV infection induces the formation of stress granules in several mammalian cells**
716 HepG2 or CMMT cells were infected with Asibi at MOI of 20 for, respectively, 48 and 24 hours. Huh7
717 cells were infected with YFV-HD Dakar at MOI of 10 for 24 hours. Cells were then stained with NS4b
718 (purple), TIAR (green), G3BP (red) antibodies and NucBlue® (blue).
719
720 **Fig. 4: PKR contributes to stress granule formation in Asibi-infected Huh7 cells**
721 (**A**) Huh7 cells were left uninfected (NI) or infected with Asibi at an MOI of 20 for 24 or 48 hours.
722 Whole-cell lysates were analysed by Western blotting with antibodies against the indicated proteins.
723 Samples were loaded on the same gel. *: unspecific bands. (**B**) Whole-cell lysates of Huh7-shLuc and
724 Huh7-shPKR cells were analysed by Western blotting with antibodies against the indicated proteins.
725 (**C**) Huh7-shLuc and Huh7-shPKR cells were treated with 0.5 mM NaArs for 30 min and stained with
726 TIAR (green) and G3BP (red) antibodies, as well as with NucBlue® (blue). (**D**) Huh7 cells were left
727 uninfected (NI) or infected with YFV-Asibi at MOI of 2 or 20 for 24 or 34 hours. Cells were then stained
728 with NS4b (purple), TIAR (green), G3BP (red) antibodies and NucBlue® (blue). Images are
729 representative of two independent experiments. Percentage of G3BP-positive (**E**) or NS4b-positive cells
730 (**F**) were estimated by analysing at least 200 cells per condition. ns: non-significant, *: $p<0.05$, **:
731 $p<0.01$, ***: $p<0.001$.
732
733 **Fig. 5: PKR contributes to innate response in Asibi-infected Huh7 cells**
734 Huh7-shLuc or -shPKR cells were left uninfected (NI) or infected with Asibi at MOI of 2 or 20 for 24
735 or 34 hours. The relative amounts of (**A**) *PKR* mRNA, (**C**) *IL6* mRNA, (**D**) *TNFA* mRNA and (**E**) *IFNB*
736 mRNA were determined by qPCR analysis and normalized to that of GAPDH mRNA and non-infected
737 shLuc samples. The relative amounts of cell-associated viral RNA were determined by RT-qPCR
738 analysis (**B**) and expressed as genome equivalents (YFV-GE) per µg of total cellular RNA. Mean ± SD
739 is represented. One-way ANOVA on log transformed data with Tukey corrected multiple comparisons

740 tests were performed. shPKR samples were compared to shLuc ones. ns: non-significant, *: p<0.05, **:
741 p<0.01, ***: p<0.001.
742
743 **Fig. 6: Knock-down of G3BP1, G3BP2, TIAR and TIA1 inhibits stress granules formation**
744 (**A**) Huh7 cells were transfected with scramble siRNA (siScr) or with siRNA targeting G3BP1, G3BP2,
745 TIAR and TIA1 (siSG) 48 and 24 hours prior to Asibi infection. Transfected cells were left uninfected
746 (NI), treated with 0.5 mM NaArs for 30 min (NaArs) or infected with Asibi at MOI of 2 or 20 for 24 or
747 34 hours. Cells were then stained with NS1 (purple), eIF3b (green), eIF4G (red) antibodies and
748 NucBlue® (blue). Images are representative of two independent confocal microscopy analyses.
749 Percentages of eIF4G- and eIF3b-positive (**B**) or NS1-positive cells (**D**) were estimated. (**C**) Stress
750 granule area was determined for each cell as the sum of the whole area occupied by stress granules
751 divided by the total cell surface. (**B-D**) Around 200 cells per independent experiment were scored. ns:
752 non-significant, *: p<0.05, **: p<0.01, ***: p<0.001.
753
754 **Fig. 7: Inhibition of stress granule formation has limited effect on antiviral response**
755 Huh7 cells were transfected with scramble siRNA (siScr) or with four pools of siRNA targeting G3BP1,
756 G3BP2, TIAR and TIA1 (siSG) 48 and 24 hours prior to infection. Transfected cells were left uninfected
757 (NI) or infected with Asibi at an MOI of 2 or 20. Cells were harvested prior to infection (0 h), 24 or 34
758 hours post-infection. The relative amount of (**A**) *G3BP1* mRNA, (**B**) *G3BP2* mRNA, (**C**) *TIAR* mRNA,
759 (**D**) *TIA1* mRNA, (**F**) *IL6* mRNA, (**G**) *TNFA* mRNA and (**H**) *IFNB* mRNA was determined by qPCR
760 analysis and normalized to that of GAPDH mRNA and non-infected sh-Scr samples. The relative
761 amounts of cell-associated viral RNA were determined by RT-qPCR analysis (**E**) and expressed as
762 genome equivalents (YFV-GE) per µg of total cellular RNA. Mean ± SD is represented. One-way
763 ANOVA on log transformed data with Tukey corrected multiple comparisons test were performed.
764 Samples treated with siSG-RNA were compared to siScr samples. ns: non-significant, *: p<0.05, **:
765 p<0.01, ***: p<0.001.
766
767 **Fig. 8: RIG-I signaling is not involved in stress granule assembly**

768 (**A**) Huh7 and Huh7.5 cells were left uninfected (NI), treated with 0.5 mM NaArs for 30 min (NaArs)
769 or infected with Asibi at MOI of 2 or 20 for 24 or 34 hours. Cells were then stained with NS4b (purple),
770 TIAR (green), G3BP (red) antibodies and NucBlue® (blue). (**B-C**) Images are representative of two
771 independent confocal microscopy analyses. Around 200 cells per independent experiment were scored.
772 Percentages of G3BP-positive (**B**) or NS4b-positive cells (**C**) were estimated. ns: non-significant, *:
773 $p<0.05$, **: $p<0.01$, ***: $p<0.001$.
774
775 **Fig. 9: YFN RNA is excluded form stress granules**
776 (**A**) Huh7 cells were left uninfected (NI) or infected with Asibi at MOI of 20 for 24 hours. Cells were
777 then stained with TIAR (green) and NucBlue® (blue), prior to be processed for FISH using a probe
778 specific for YFV (+) strand RNA (red). (**B**) Huh7 cells were left untreated (NT) or treated with 0.5 mM
779 NaArs for 30 min. Cells were then stained with RIG-I (purple), TIAR (green) antibodies and NucBlue®
780 (blue).
781

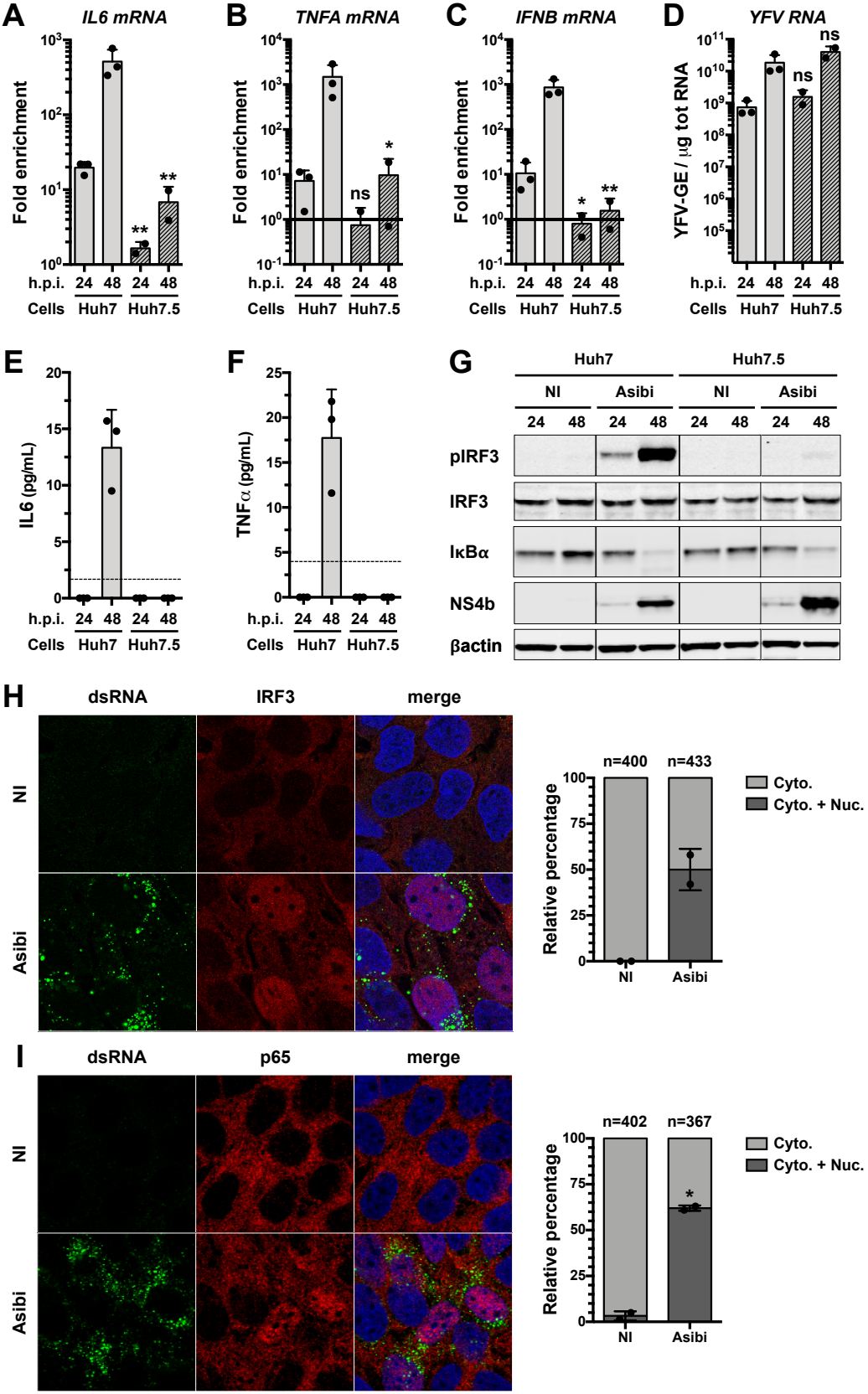
A
IL6 mRNA
Fold enrichment
h.p.i. 24 48 24 48
Cells Huh7 Huh7.5
B
TNFA mRNA
Fold enrichment
ns
C
IFNB mRNA
Fold enrichment
D
YFV RNA
YFV-GE / µg tot RNA
ns
E
IL6 (pg/mL)
F
TNFα (pg/mL)
G
Huh7
Huh7.5
NI
Asibi
pIRF3
IRF3
IκBα
NS4b
βactin
H
dsRNA
IRF3
merge
NI
Asibi
n=400
n=433
Relative percentage
Cyto.
Cyto. + Nuc.
I
dsRNA
p65
merge
n=402
n=367

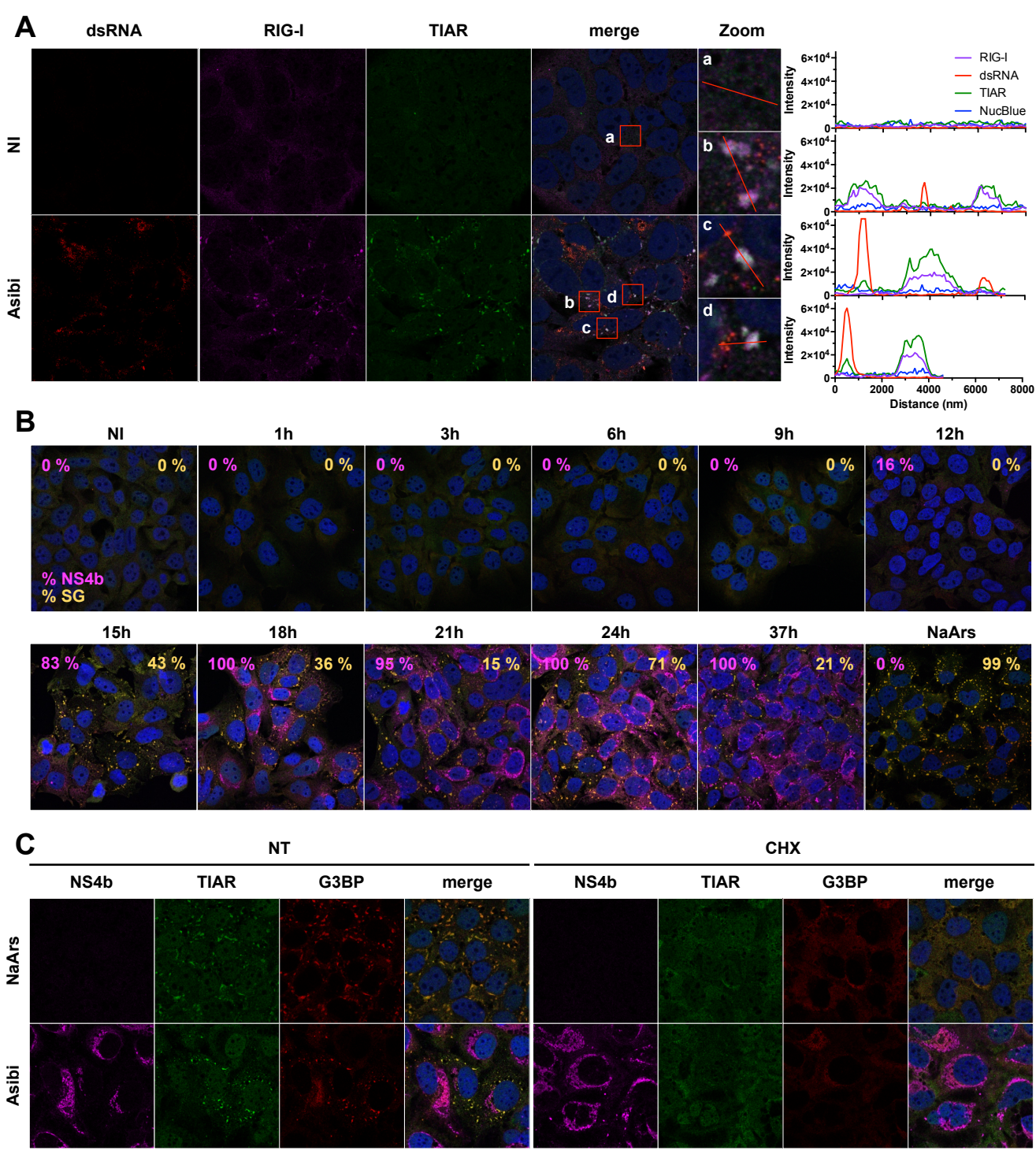
A
dsRNA
RIG-I
TIAR
merge
Zoom
NI
Asibi
a
b
c
d
RIG-I
dsRNA
TIAR
NucBlue
Intensity
Distance (nm)
B
NI
1h
3h
6h
9h
12h
15h
18h
21h
24h
37h
NaArs
% NS4b
% SG
C
NT
CHX
NS4b
TIAR
G3BP
merge
NaArs
Asibi

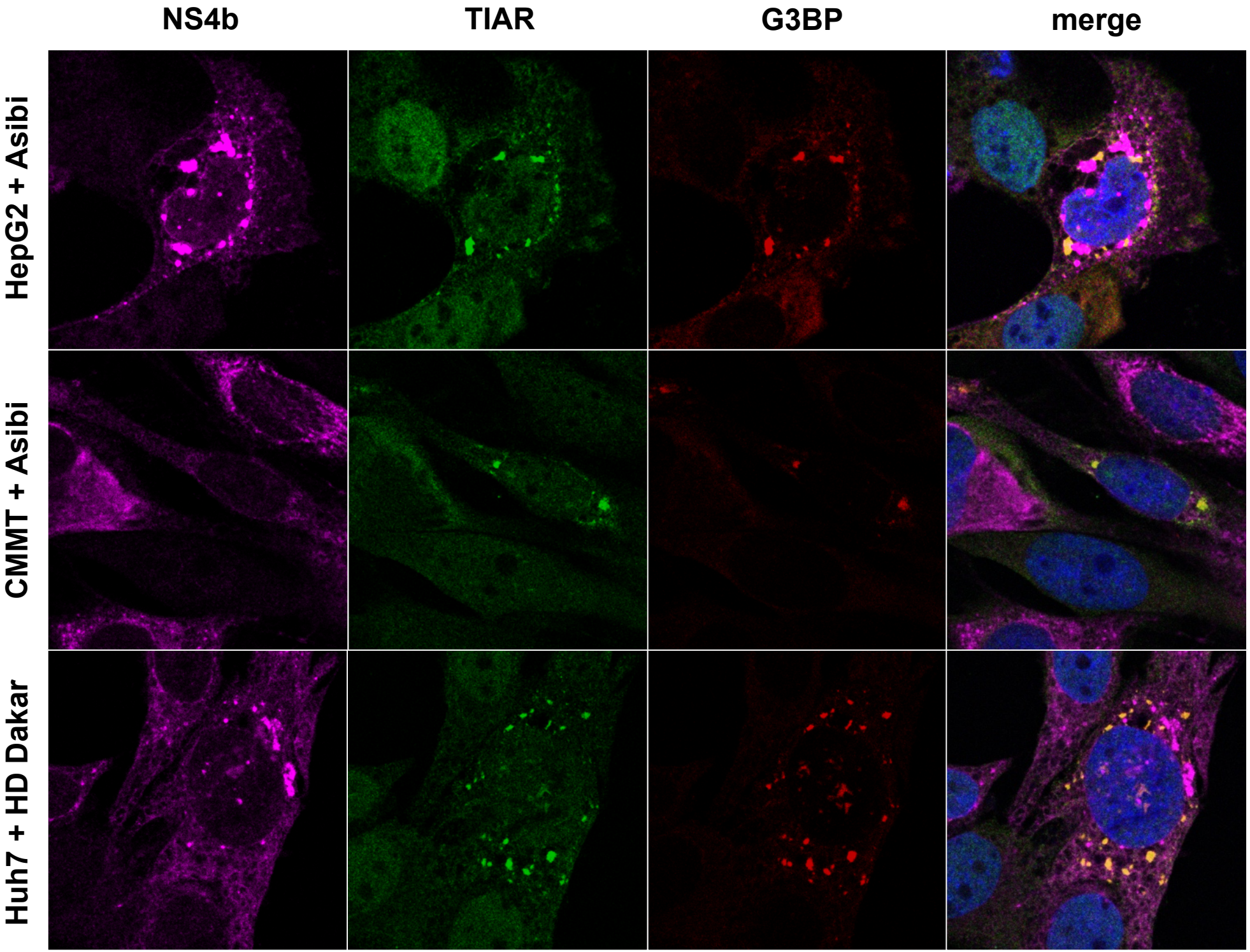
NS4b
TIAR
G3BP
merge
HepG2 + Asibi
CMMT + Asibi
Huh7 + HD Dakar

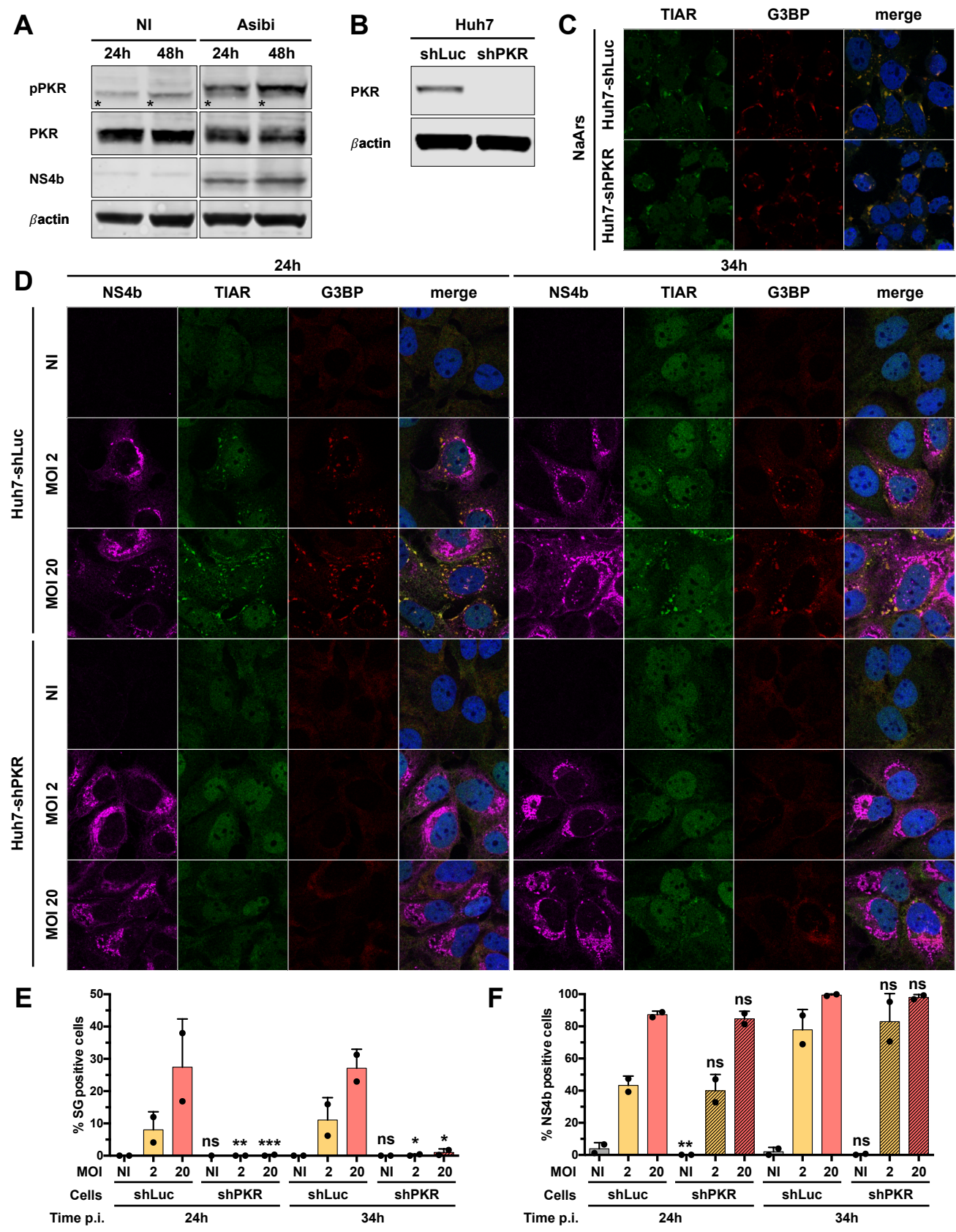
A
NI
Asibi
24h
48h
24h
48h
pPKR
PKR
NS4b
βactin
B
Huh7
shLuc
shPKR
PKR
βactin
C
TIAR
G3BP
merge
NaArs
Huh7-shLuc
Huh7-shPKR
D
24h
34h
NS4b
TIAR
G3BP
merge
Huh7-shLuc
Huh7-shPKR
NI
MOI 2
MOI 20
E
% SG positive cells
MOI
Cells
Time p.i.
shLuc
shPKR
24h
34h
ns
**
***
*
F
% NS4b positive cells
MOI
Cells
Time p.i.
shLuc
shPKR
24h
34h
ns
**

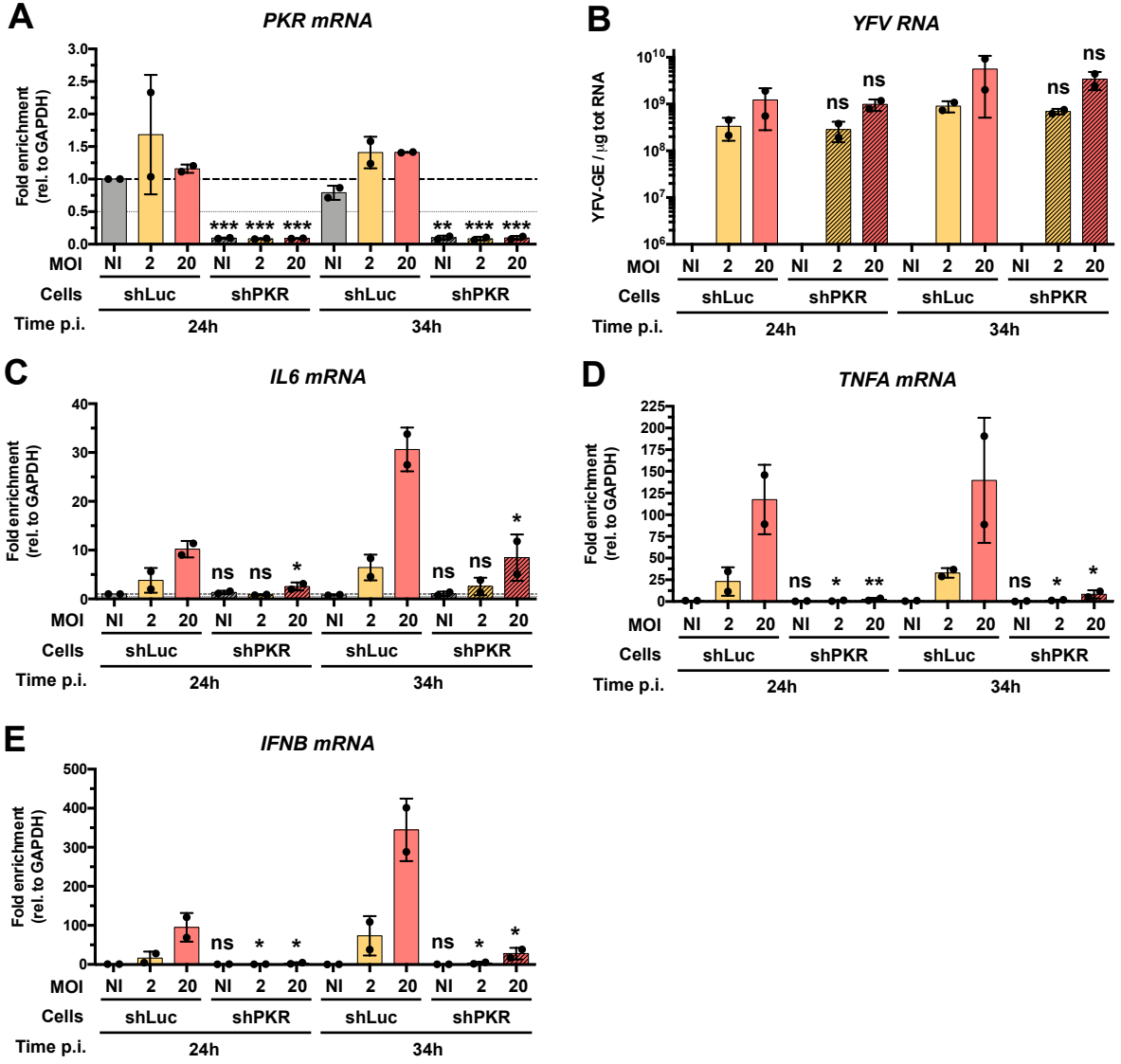
A
PKR mRNA
Fold enrichment (rel. to GAPDH)
3.0
2.5
2.0
1.5
1.0
0.5
0.0
***
***
***
**
***
***
MOI
NI
2
20
Cells
shLuc
shPKR
Time p.i.
24h
34h
B
YFV RNA
YFV-GE / µg tot RNA
10^{10}
10^{9}
10^{8}
10^{7}
10^{6}
ns
C
IL6 mRNA
40
30
20
10
0
*
D
TNFA mRNA
225
200
175
150
125
100
75
50
25
0
**
E
IFNB mRNA
500
400
300
200
100
0

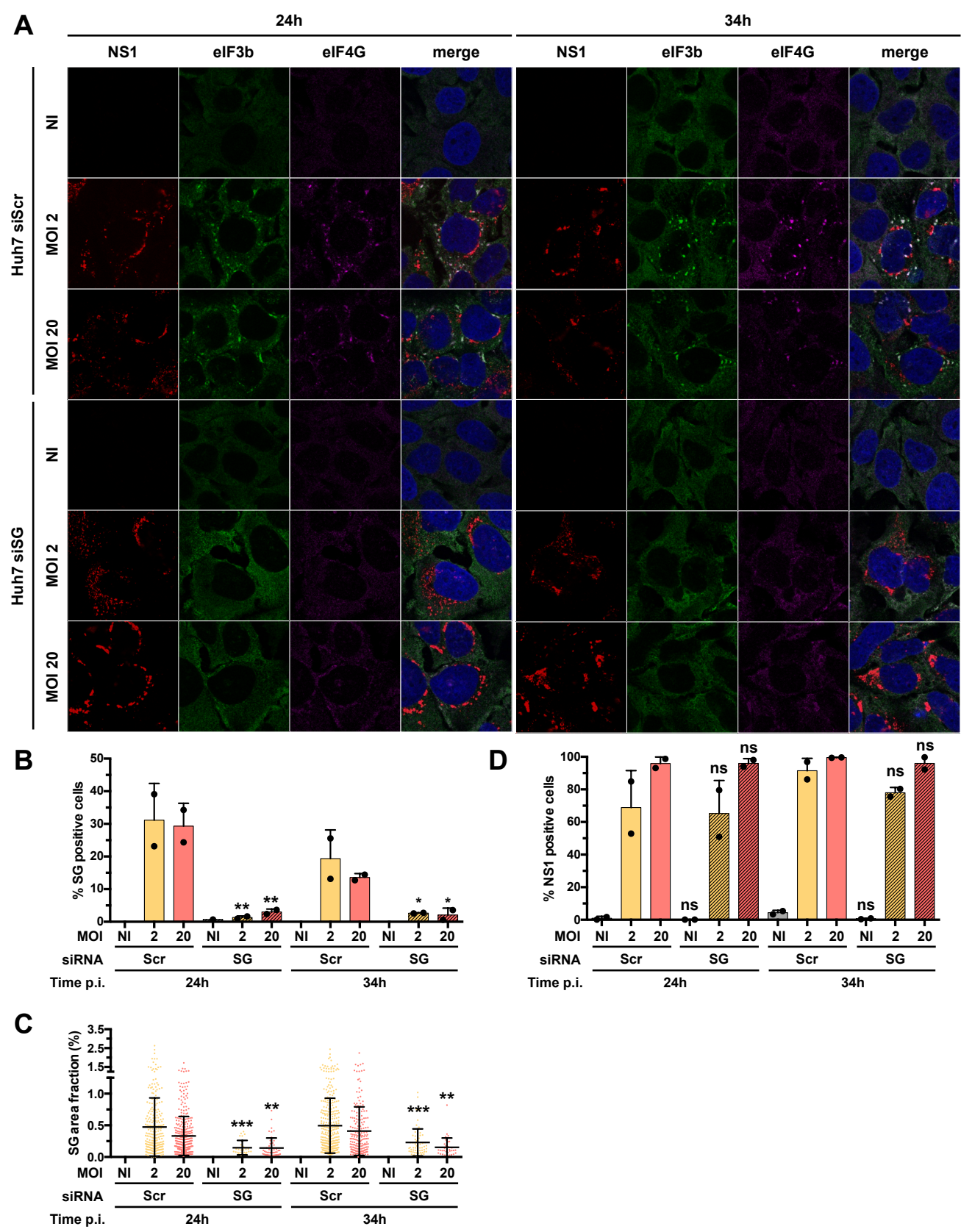
A
24h
34h
NS1
eIF3b
eIF4G
merge
Huh7 siScr
Huh7 siSG
NI
MOI 2
MOI 20
B
% SG positive cells
MOI
siRNA
Scr
SG
Time p.i.
24h
34h
C
SG area fraction (%)
D
% NS1 positive cells
ns

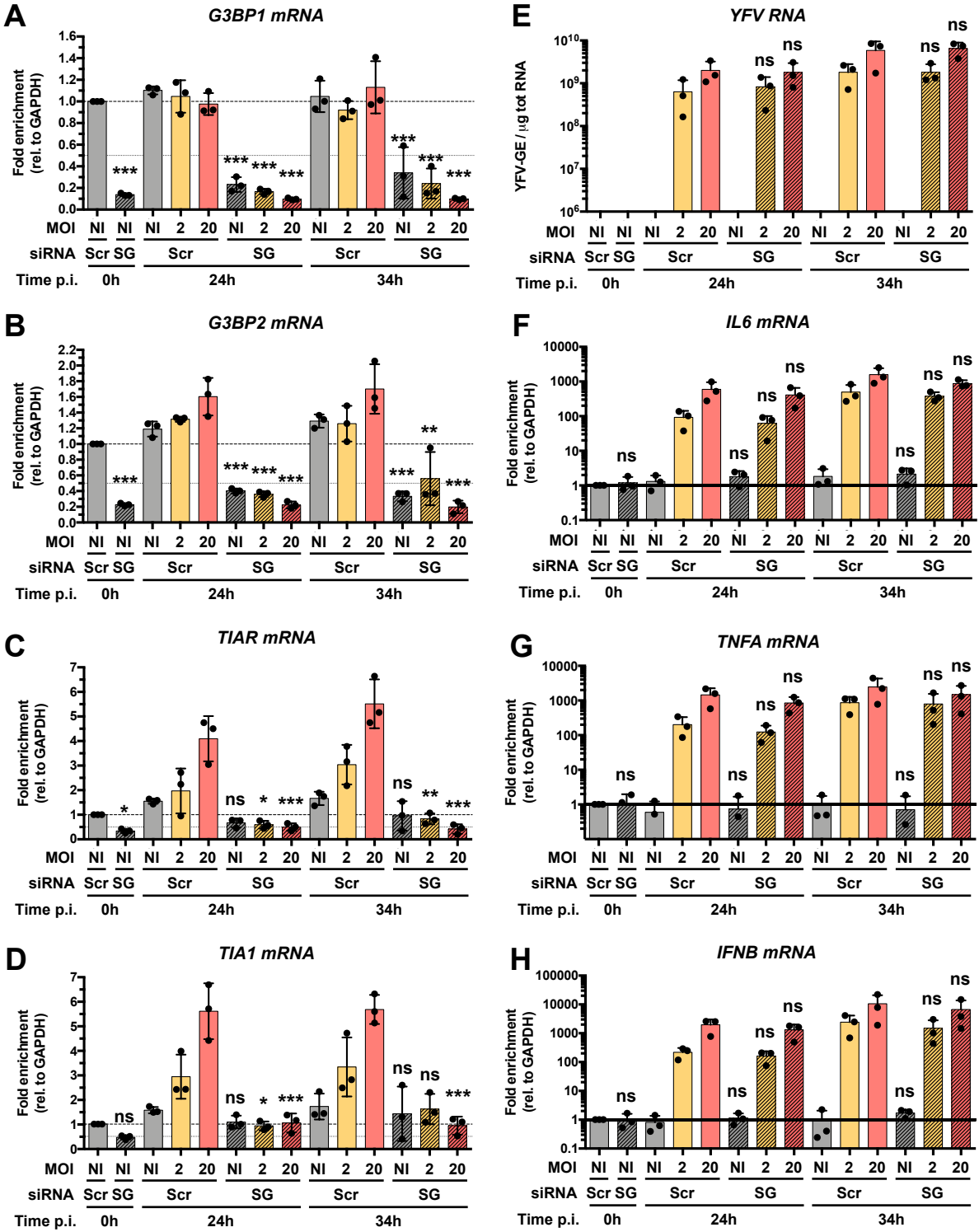
A
G3BP1 mRNA
Fold enrichment (rel. to GAPDH)
B
G3BP2 mRNA
C
TIAR mRNA
D
TIA1 mRNA
E
YFV RNA
YFV-GE / µg tot RNA
F
IL6 mRNA
G
TNFA mRNA
H
IFNB mRNA
MOI NI NI NI 2 20 NI 2 20 NI 2 20 NI 2 20
siRNA Scr SG Scr SG Scr SG
Time p.i. 0h 24h 34h
ns
*
**
***

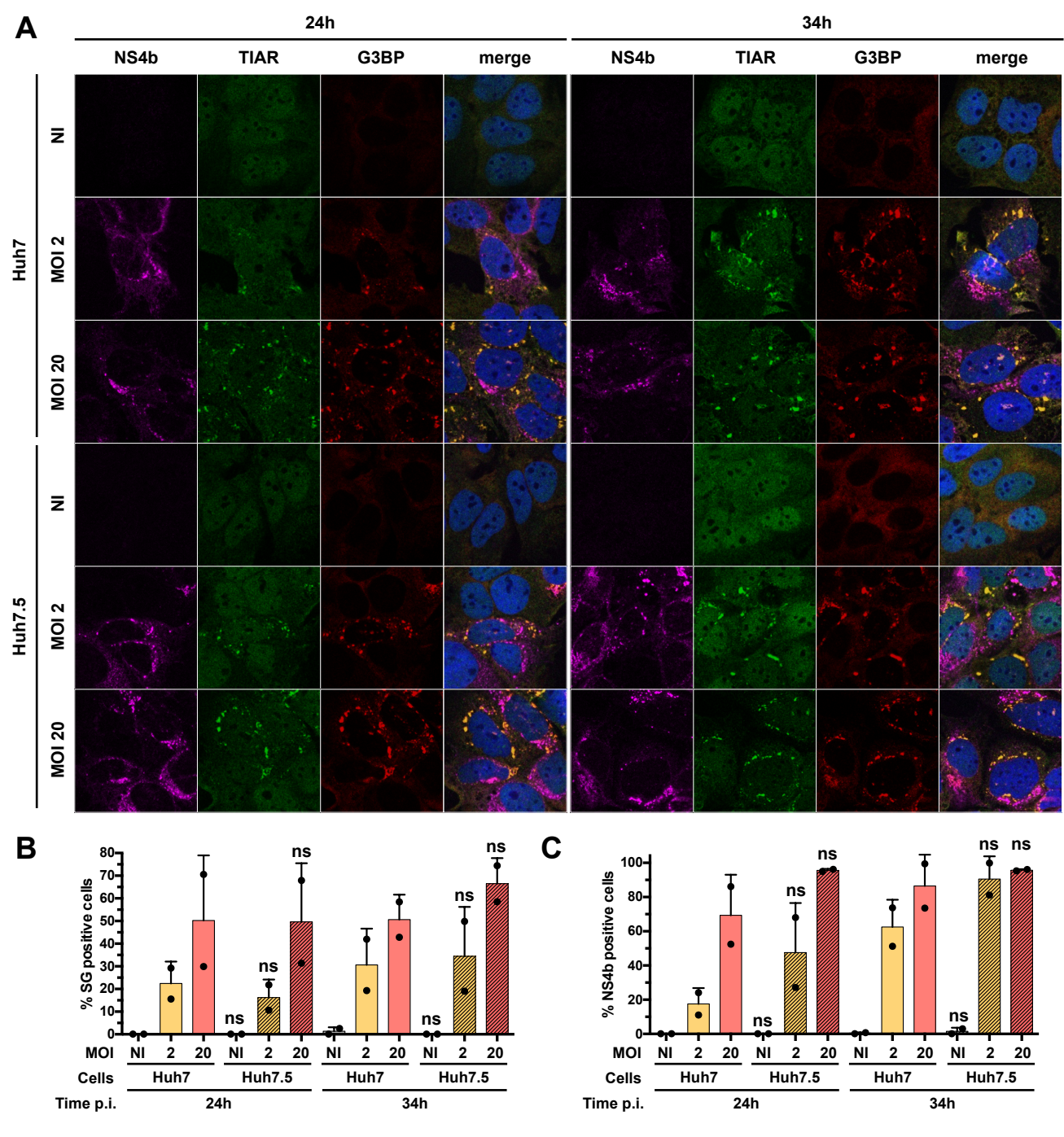
A
24h
34h
NS4b
TIAR
G3BP
merge
Huh7
Huh7.5
NI
MOI 2
MOI 20
B
% SG positive cells
ns
MOI
NI
2
20
Cells
Huh7
Huh7.5
Time p.i.
24h
34h
C
% NS4b positive cells

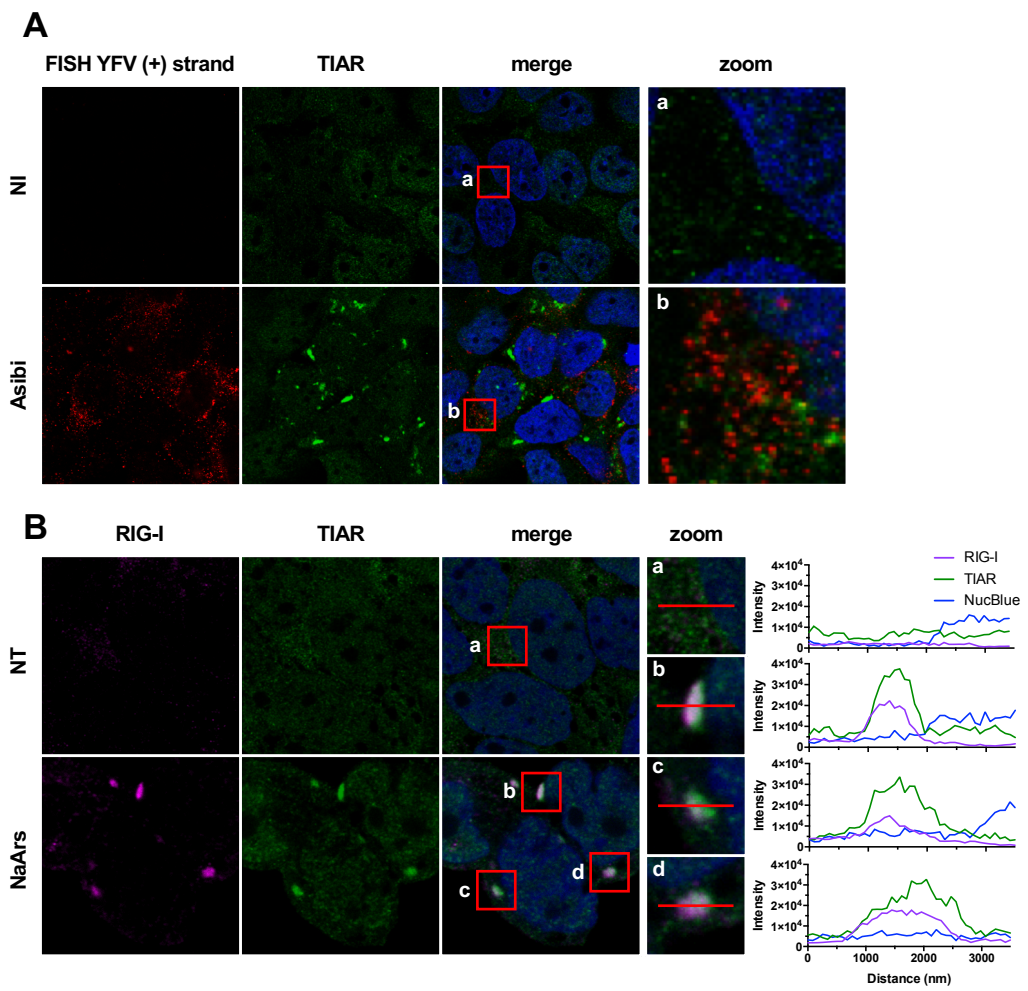
A
FISH YFV (+) strand
TIAR
merge
zoom
NI
Asibi
a
b
B
RIG-I
TIAR
merge
zoom
NT
NaArs
a
b
c
d
RIG-I
TIAR
NucBlue
Intensity
4×10⁴
3×10⁴
2×10⁴
1×10⁴
0
1000
2000
3000
Distance (nm)